Two families of explicit models constructed from a homogenization solution for the magnetoelastic response of MREs containing iron and ferrofluid particles

Victor Lefèvre, Kostas Danas, Oscar Lopez-Pamis

Two families of explicit models constructed from a homogenization solution for the magnetoelastic response of MREs containing iron and ferrofluid particles

Victor Lefèvre[a], Kostas Danas[b], Oscar Lopez-Pamies[c]

[a] *Department of Mechanical Engineering, Northwestern University, Evanston, IL 60208, USA*
[b] *LMS, C.N.R.S, École Polytechnique, Institute Polytechnique de Paris, Palaiseau, 91128, France*
[c] *Department of Civil and Environmental Engineering, University of Illinois, Urbana–Champaign, IL 61801, USA*

Abstract

This work puts forth two families of fully explicit continuum or phenomenological models that are constructed by approximating an analytical (but implicit) homogenization solution recently derived for the free-energy function describing the macroscopic magnetoelastic response of two classes of MREs comprised of an isotropic incompressible elastomer filled with a random isotropic distribution of: *i*) spherical iron particles and *ii*) spherical ferrofluid particles. Both families are given in terms of free-energy functions $W^H = W^H(\mathbf{F}, \mathbf{H})$ that depend on the deformation gradient $\mathbf{F}$ and the Lagrangian magnetic field $\mathbf{H}$ and are constructed so as to agree identically with the homogenization solution for small and large applied magnetic fields, this for arbitrary finite deformations and arbitrary volume fractions c of particles in the entire physical range $c \in [0, 1]$. The accuracy of the proposed phenomenological models is assessed *inter alia* via the direct comparison of their predictions with that of the homogenization solution for a boundary-value problem of both fundamental and practical significance: the magnetostriction response of a spherical MRE specimen subject to a remotely applied uniform magnetic field.

Key words: Magnetorheological elastomers; Ferrofluid inclusions; Magnetostriction; Finite magnetoelastostatics

1. Introduction

The purpose of this paper is to introduce two families of fully explicit free-energy functions to describe the macroscopic magnetoelastic response of two classes of isotropic MREs (magnetorheological elastomers) under arbitrary finite deformations and finite magnetic fields. The first class is a conventional one, that is, the MREs are comprised of an isotropic incompressible elastomer filled with a random isotropic distribution of spherical iron particles. The second class corresponds to a new class of MREs that have been only recently introduced theoretically (Lefèvre et al., 2017): those comprised of an isotropic incompressible elastomer filled with a random isotropic distribution of spherical ferrofluid[1] particles. The proposed free-energy functions are constructed by approximating an analytical homogenization solution recently put forth in (Lefèvre et al., 2017) for such two classes[2] of MREs; while analytical in form, the solution of Lefèvre et al. (2017) is implicit

Email addresses: victor.lefevre@northwestern.edu (Victor Lefèvre), konstantinos.danas@polytechnique.edu (Kostas Danas), pamies@illinois.edu (Oscar Lopez-Pamies)

[1] As opposed to the conventional iron particles, ferrofluid particles are highly deformable. It is this high deformability that imparts superior properties to the resulting MREs; see Section 6 in (Lefèvre et al., 2017).

[2] The full version of the solution of Lefèvre et al. (2017) applies to $N = 2$ and 3 space dimensions and any arbitrary isotropic suspension of magnetizable particles; this includes particles of any shapes that may appear isolated or in clusters, so long as the microstructure is isotropic. The focus of this work is on the practically prominent case of particles that are made of iron or ferrofluid and are spherical in shape.

in that one nonlinear algebraic equation, dependent on the material properties of the elastomeric matrix and particles and on the applied deformation and magnetic field, needs to be solved numerically for its evaluation.

It is by now plain that the construction of purely continuum or phenomenological (i.e., top-down) models to describe and predict the macroscopic magnetoelastic response of MREs is likely to remain difficult because of the challenges of carrying out experiments that probe their material (and *not* structural) behavior over a meaningful range of deformations and magnetic fields. On the other hand, the construction of full-blown homogenization (i.e., bottom-up) models to describe and predict the macroscopic magnetoelastic response of MREs is likely to remain of little practical use because of the computational costs associated with their deployment to solve macroscopic boundary-value problems; nevertheless, homogenization-based approaches are expected to be very useful to understand key microscopic mechanisms; see, e.g., Keip and Rambausek (2015); Danas (2017); Lefèvre et al. (2017). In this context, the free-energy functions proposed in this paper can be thought of as a necessary compromise between the two approaches. Indeed, the proposed free-energy functions can be viewed as phenomenological (top-down) models that are easy to implement numerically to solve boundary-value problems and that, at the same time, are grounded on rigorous homogenization (bottom-up) results and hence are expected to be descriptive and predictive of actual MREs.

The paper is organized as follows. We begin in Section 2 by introducing notation and by recalling the basic equations for the continuum modeling of magnetoelastic solids. In Section 3, we spell out the homogenization solution of Lefèvre et al. (2017) for the case of MREs containing iron particles and recall some of its key theoretical and practical features. We devote Section 4 to the construction of the family of explicit free-energy functions for such a class of MREs. In an entirely analogous manner, we spell out in Section 5 the homogenization solution of Lefèvre et al. (2017) for the case of MREs containing ferrofluid particles and then present in Section 6 a family of explicit free-energy functions for that new class of MREs. We devote Section 7 to assessing the two families of proposed models via direct comparisons with the homogenization solution. These include comparisons between the predictions generated by the proposed models with those generated by homogenization solution for the magnetostriction response of spherical MRE specimens subject to a remotely applied uniform magnetic field.

2. Preliminaries

Kinematics. Consider a deformable and magnetizable homogeneous solid that occupies in its initial configuration a bounded domain $\Omega_0 \subset \mathbb{R}^3$, with boundary $\partial\Omega_0$ and unit outward normal $\mathbf{N}$. We identify material points by their initial position vector $\mathbf{X} \in \Omega_0$. Due to externally applied stimuli to be described below, the position vector $\mathbf{X}$ of a material point moves to a new position specified by $\mathbf{x} = \mathbf{y}(\mathbf{X})$, where $\mathbf{y}$ is a mapping from Ω_0 to the current configuration Ω, also contained in $\mathbb{R}^3$. We consider only invertible deformations, and write the deformation gradient at $\mathbf{X}$ as

$$\mathbf{F}(\mathbf{X}) = \operatorname{Grad} \mathbf{y}.$$

Constitutive behavior. Absent dissipation effects, the constitutive behavior of the solid is taken to be characterized by a thermodynamic potential that describes how the solid stores energy through deformation and magnetization. We find it convenient to make use of thermodynamic potentials corresponding to "total" free-energy functions which combine the mechanical and the magnetic contributions (Dorfmann and Ogden, 2004). Two versions of this are particularly useful:

- *The* $(\mathbf{F}, \mathbf{H})$ *formulation.* This case corresponds to making use of a free-energy function

$$W^H = W^H(\mathbf{F}, \mathbf{H}), \tag{1}$$

  where the Lagrangian magnetic field $\mathbf{H}$ plays the role of the independent magnetic variable. In terms of (1), the total first Piola-Kirchhoff stress tensor $\mathbf{S}$ and the Lagrangian magnetic induction $\mathbf{B}$ at any material point $\mathbf{X} \in \Omega_0$ are simply given by the relations

$$\mathbf{S}(\mathbf{X}) = \frac{\partial W^H}{\partial \mathbf{F}}(\mathbf{F}, \mathbf{H}) \qquad \text{and} \qquad \mathbf{B}(\mathbf{X}) = -\frac{\partial W^H}{\partial \mathbf{H}}(\mathbf{F}, \mathbf{H}). \tag{2}$$

- *The* $(\mathbf{F},\mathbf{B})$ *formulation.* This case corresponds to making use of a free-energy function

$$W^B = W^B(\mathbf{F},\mathbf{B}), \tag{3}$$

where the Lagrangian magnetic induction $\mathbf{B}$, instead of $\mathbf{H}$, plays the role of the independent magnetic variable. In terms of (3), we have the constitutive relations

$$\mathbf{S}(\mathbf{X}) = \frac{\partial W^B}{\partial \mathbf{F}}(\mathbf{F},\mathbf{B}) \qquad \text{and} \qquad \mathbf{H}(\mathbf{X}) = \frac{\partial W^B}{\partial \mathbf{B}}(\mathbf{F},\mathbf{B}). \tag{4}$$

Remark 1. If a given free-energy function (1) is concave in its second argument, it follows that (3) is its partial Legendre transform. Precisely,

$$W^B(\mathbf{F},\mathbf{B}) = (W^H)^*(\mathbf{F},\mathbf{B}) = \sup_{\mathbf{H}} \left\{\mathbf{B}\cdot\mathbf{H} + W^H(\mathbf{F},\mathbf{H})\right\}. \tag{5}$$

By the same token, if a given free-energy function (3) is convex in its second argument, (1) is its partial Legendre transform:

$$W^H(\mathbf{F},\mathbf{H}) = (W^B)^*(\mathbf{F},\mathbf{H}) = -\sup_{\mathbf{B}} \left\{\mathbf{B}\cdot\mathbf{H} - W^B(\mathbf{F},\mathbf{B})\right\}. \tag{6}$$

Remark 2. The total Cauchy stress $\boldsymbol{\sigma}$, Eulerian magnetic field $\mathbf{h}$, and Eulerian magnetic induction $\mathbf{b}$ at the position $\mathbf{x}\in\Omega$ occupied by the material point $\mathbf{X}$ in the deformed configuration are given in terms of their Lagrangian counterparts by the relations

$$\boldsymbol{\sigma}(\mathbf{x}) = \frac{1}{\det\mathbf{F}}\mathbf{S}\mathbf{F}^T, \qquad \mathbf{h}(\mathbf{x}) = \mathbf{F}^{-T}\mathbf{H}, \qquad \mathbf{b}(\mathbf{x}) = \frac{1}{\det\mathbf{F}}\mathbf{F}\mathbf{B}. \tag{7}$$

Moreover, the magnetization $\mathbf{m}$ (per unit deformed volume) at any $\mathbf{x}\in\Omega$ is given by

$$\mathbf{m}(\mathbf{x}) = \frac{1}{\mu_0}\mathbf{b} - \mathbf{h}, \tag{8}$$

where $\mu_0 = 4\pi\times 10^{-7}$ H/m stands for the permeability of vacuum.

Remark 3. For isotropic solids, the case of interest in this paper, the free-energy function (1) admits the representation

$$W^H(\mathbf{F},\mathbf{H}) = W^H(I_1, I_2, J, I_4^H, I_5^H, I_6^H) \tag{9}$$

in terms of the six standard invariants

$$I_1 = \operatorname{tr}\mathbf{C}, \qquad I_2 = \frac{1}{2}\left[(\operatorname{tr}\mathbf{C})^2 - \operatorname{tr}\mathbf{C}^2\right], \qquad J = \det\mathbf{F}, \tag{10}$$

and

$$I_4^H = \mathbf{H}\cdot\mathbf{H}, \qquad I_5^H = \mathbf{H}\cdot\mathbf{C}^{-1}\mathbf{H}, \qquad I_6^H = \mathbf{H}\cdot\mathbf{C}^{-2}\mathbf{H}, \tag{11}$$

where $\mathbf{C} = \mathbf{F}^T\mathbf{F}$ stands for the right Cauchy-Green deformation tensor and where, for convenience, we have maintained the same label W^H in the right-hand side of (9) in order not to introduce separate notation; see, e.g., Steigmann (2004) and Dorfmann and Ogden (2004).

Similarly, the free-energy function (3) admits the representation

$$W^B(\mathbf{F},\mathbf{B}) = W^B(I_1, I_2, J, I_4^B, I_5^B, I_6^B)$$

in terms of (10) and the invariants

$$I_4^B = \mathbf{B}\cdot\mathbf{B}, \qquad I_5^B = \mathbf{B}\cdot\mathbf{C}\mathbf{B}, \qquad I_6^B = \mathbf{B}\cdot\mathbf{C}^2\mathbf{B}. \tag{12}$$

Boundary conditions and source terms. We now specify the external stimuli applied to the solid, which comprise both prescribed magnetic and mechanical boundary data and mechanical source terms in the bulk.

Magnetically, consistent with the manner in which magnetic fields are applied in practice, we take that the solid is immersed in a surrounding space (e.g., air) where there is a heterogeneous magnetic field $\overline{\mathbf{H}}(\mathbf{X})$ and corresponding magnetic induction $\overline{\mathbf{B}}(\mathbf{X})$ that result by the nearby presence of permanent magnets and/or electromagnets and by the interaction of these with the solid and possibly other magnetizable bodies. We then have the boundary condition

$$\mathbf{H}\times\mathbf{N}=\overline{\mathbf{H}}\times\mathbf{N},\quad \mathbf{X}\in\partial\Omega_0 \tag{13}$$

or, equivalently,

$$\mathbf{B}\cdot\mathbf{N}=\overline{\mathbf{B}}\cdot\mathbf{N},\quad \mathbf{X}\in\partial\Omega_0 \tag{14}$$

over the entirety of the boundary of the domain occupied by the solid.

Mechanically, on a portion $\partial\Omega_0^{\mathcal{D}}$ of the boundary $\partial\Omega_0$, the deformation field $\mathbf{y}$ is taken to be given by a known function $\overline{\mathbf{y}}(\mathbf{X})$, while the complementary part of the boundary $\partial\Omega_0^{\mathcal{N}}=\partial\Omega_0\setminus\partial\Omega_0^{\mathcal{D}}$ is subjected to a prescribed mechanical traction $\overline{\mathbf{t}}(\mathbf{X})$. Precisely,

$$\mathbf{y}=\overline{\mathbf{y}},\quad \mathbf{X}\in\partial\Omega_0^{\mathcal{D}}\qquad\text{and}\qquad \mathbf{S}\mathbf{N}=\overline{\mathbf{t}}+\mathbf{S}_M\mathbf{N},\quad \mathbf{X}\in\partial\Omega_0^{\mathcal{N}}. \tag{15}$$

In this last expression, $\mathbf{S}_M$ stands for the Maxwell stress outside of the solid; see, e.g., Kankanala and Triantafyllidis (2004) and Dorfmann and Ogden (2004). In the case when the solid is surrounded by air,

$$\mathbf{S}_M=\mathbf{F}^{-T}\overline{\mathbf{H}}\otimes\overline{\mathbf{B}}-\frac{J\mu_0}{2}\left(\mathbf{F}^{-T}\overline{\mathbf{H}}\cdot\mathbf{F}^{-T}\overline{\mathbf{H}}\right)\mathbf{F}^{-T},$$

where $\overline{\mathbf{B}}=\mu_0 J\mathbf{F}^{-1}\mathbf{F}^{-T}\overline{\mathbf{H}}$ and where we emphasize that the meaning of the deformation gradient $\mathbf{F}$ in the air needs to be interpreted appropriately; see Subsection 7.2 below.

Throughout Ω_0, we also consider that the solid is subjected to a body force

$$\mathbf{f}(\mathbf{X}),\quad \mathbf{X}\in\Omega_0. \tag{16}$$

Governing equations. Absent inertia and in the context of magnetostatics, the relevant equations of balance of linear and angular momenta read as

$$\operatorname{Div}\mathbf{S}=\mathbf{0}\qquad\text{and}\qquad \mathbf{S}\mathbf{F}^T=\mathbf{F}\mathbf{S}^T,\quad \mathbf{X}\in\Omega_0 \tag{17}$$

while the relevant equations of Maxwell read as

$$\operatorname{Div}\mathbf{B}=0\qquad\text{and}\qquad \operatorname{Curl}\mathbf{H}=\mathbf{0},\quad \mathbf{X}\in\mathbb{R}^3. \tag{18}$$

When using the free-energy function (1) as the constitutive input, the balance of angular momentum $(17)_2$ can be automatically satisfied by enforcing material frame indifference — that is, by making use of free-energy functions such that $W^H(\mathbf{Q}\mathbf{F},\mathbf{H})=W^H(\mathbf{F},\mathbf{H})$ for all $\mathbf{Q}\in Orth^+$ and arbitrary $\mathbf{F}$ and $\mathbf{H}$ — while Ampère's law $(18)_2$ can also be automatically satisfied by introducing a scalar potential ψ such that $\mathbf{H}=-\operatorname{Grad}\psi$. It then follows that the governing equations for the solid reduce to the following coupled system of boundary-value problems:

$$\begin{cases}\operatorname{Div}\left[\dfrac{\partial W^H}{\partial\mathbf{F}}(\mathbf{F},\mathbf{H})\right]+\mathbf{f}(\mathbf{X})=\mathbf{0},\quad \mathbf{X}\in\Omega_0\\ \mathbf{y}(\mathbf{X})=\overline{\mathbf{y}}(\mathbf{X}),\quad \mathbf{X}\in\partial\Omega_0^{\mathcal{D}}\\ \left(\left[\dfrac{\partial W^H}{\partial\mathbf{F}}(\mathbf{F},\mathbf{H})\right]-\mathbf{S}_M\right)\mathbf{N}=\overline{\mathbf{t}}(\mathbf{X}),\quad \mathbf{X}\in\partial\Omega_0^{\mathcal{N}}\end{cases}\qquad\text{and}\qquad \begin{cases}\operatorname{Div}\left[\dfrac{\partial W^H}{\partial\mathbf{H}}(\mathbf{F},\mathbf{H})\right]=0,\quad \mathbf{X}\in\Omega_0\\ \left[\dfrac{\partial W^H}{\partial\mathbf{H}}(\mathbf{F},\mathbf{H})\right]\cdot\mathbf{N}=\overline{\mathbf{B}}\cdot\mathbf{N},\quad \mathbf{X}\in\partial\Omega_0\end{cases} \tag{19}$$

for the deformation field $\mathbf{y}(\mathbf{X})$ and the scalar magnetic potential $\psi(\mathbf{X})$.

On the other hand, when using the free-energy function (3) as the constitutive input, the balance of angular momentum $(17)_2$ can also be automatically satisfied by enforcing material frame indifference — in this case, $W^B(\mathbf{QF},\mathbf{B}) = W^B(\mathbf{F},\mathbf{B})$ for all $\mathbf{Q} \in Orth^+$ and arbitrary $\mathbf{F}$ and $\mathbf{B}$ — while Gauss law $(18)_1$ can be automatically satisfied by introducing a vector potential $\mathbf{A}$ such that $\mathbf{B} = \operatorname{Curl}\mathbf{A}$. In this case, the governing equations for the solid reduce to the coupled system of boundary-value problems

$$\left\{\begin{array}{l} \operatorname{Div}\left[\dfrac{\partial W^B}{\partial \mathbf{F}}(\mathbf{F},\mathbf{B})\right] + \mathbf{f}(\mathbf{X}) = \mathbf{0}, \quad \mathbf{X}\in\Omega_0 \\ \mathbf{y}(\mathbf{X}) = \overline{\mathbf{y}}(\mathbf{X}), \quad \mathbf{X}\in\partial\Omega_0^{\mathcal{D}} \\ \left(\left[\dfrac{\partial W^B}{\partial \mathbf{F}}(\mathbf{F},\mathbf{B})\right] - \mathbf{S}_M\right)\mathbf{N} = \overline{\mathbf{t}}(\mathbf{X}), \quad \mathbf{X}\in\partial\Omega_0^{\mathcal{N}} \end{array}\right. \quad \text{and} \quad \left\{\begin{array}{l} \operatorname{Curl}\left[\dfrac{\partial W^B}{\partial \mathbf{B}}(\mathbf{F},\mathbf{B})\right] = \mathbf{0}, \quad \mathbf{X}\in\Omega_0 \\ \left[\dfrac{\partial W^B}{\partial \mathbf{B}}(\mathbf{F},\mathbf{B})\right]\times\mathbf{N} = \overline{\mathbf{H}}\times\mathbf{N}, \quad \mathbf{X}\in\partial\Omega_0 \end{array}\right. \tag{20}$$

for the deformation field $\mathbf{y}(\mathbf{X})$ and the vector magnetic potential $\mathbf{A}(\mathbf{X})$.

Remark 4. In general, the boundary data $\overline{\mathbf{B}}$ and $\overline{\mathbf{H}}$ in $(19)_2$ and $(20)_2$ are not known *a priori*. This is because they are implicitly defined by the solution of Maxwell equations (18) in $\mathbb{R}^3\backslash\Omega_0$.

Remark 5. Schemes for generating numerical solutions for equations (19) with air occupying the surrounding space $\mathbb{R}^N\backslash\Omega_0$ have been proposed over the past few years based on the finite-element method for $N=2$ (Keip and Rambausek, 2015) and $N=3$ (Saxena et al., 2015; Pelteret et al., 2016; Lefèvre et al., 2017) space dimensions and also based on a coupled finite-element/boundary-element approach (Nedjar, 2017); see also Vu and Steinmann (2010, 2012). To our knowledge, analogous schemes for equations (20) have not yet been reported in the literature for $N=3$ spatial dimensions; see, e.g., Psarra et al. (2017) for an implementation in $N=2$ spatial dimensions. This may be partly due to the difficulty of dealing with the non-uniqueness in the definition of $\mathbf{A}$ and the additional computational cost of $\mathbf{A}$ being a vectorial — as opposed to a scalar — unknown.

3. The homogenization solution of Lefèvre et al. (2017) for MREs containing iron particles

By leveraging recent advances in iterative, comparison-medium, and computational homogenization techniques (Lopez-Pamies, 2010a; Lopez-Pamies et al., 2013; Lopez-Pamies, 2014; Lefèvre et al., 2019), Lefèvre and Lopez-Pamies (2017a,b) worked out a homogenization solution for the free-energy function describing the elastic dielectric response of dielectric elastomer composites with a large class of particulate microstructures. By leveraging in turn the mathematical analogy between electroelastostatics and magnetoelastostatics, Lefèvre et al. (2017) transcribed that solution into a homogenization solution for the free-energy function W^H describing the magnetoelastic response of a large class of isotropic MREs.

For the case of MREs comprised of an isotropic incompressible elastomer filled with a random isotropic distribution of spherical iron particles, the solution of Lefèvre et al. (2017) reads as

$$W^H(\mathbf{F},\mathbf{H}) = \begin{cases} W^H(I_1,I_4^H,I_5^H) = (1-c)\Psi_{\mathtt{m}}(\mathcal{I}_1) - c\,\mathcal{S}_{\mathtt{p}}(\mathcal{I}_5) + \dfrac{c\,\xi}{2}\mathcal{I}_5 + \dfrac{1}{2}\left(\omega(\xi)-\nu(\xi)\right)I_4^H - \dfrac{\omega(\xi)}{2}I_5^H & \text{if} \quad J=1 \\ +\infty & \text{otherwise} \end{cases}. \tag{21}$$

In this expression, $c\in[0,1]$ denotes the volume fraction of iron particles,

$$\mathcal{I}_1 = \frac{I_1-3}{(1-c)^{7/2}} + 3,$$
$$\mathcal{I}_5 = -\frac{54c(1-c)(\xi-\mu_0)\mu_0^2}{5[(2+c)\mu_0+(1-c)\xi]^3}I_4^H + \frac{9[(10-c+6c^2)\mu_0+(5+c-6c^2)\xi]\mu_0^2}{5[(2+c)\mu_0+(1-c)\xi]^3}I_5^H,$$

$$\nu(\xi) = \mu_0 + \frac{3c\mu_0(\xi-\mu_0)}{[(2+c)\mu_0+(1-c)\xi]},$$
$$\omega(\xi) = \mu_0 + \frac{3c(10+2c+3c^2)(\xi-\mu_0)\mu_0^2}{5[(2+c)\mu_0+(1-c)\xi]^2} + \frac{3c(1-c)(5+3c)(\xi-\mu_0)\mu_0\xi}{5[(2+c)\mu_0+(1-c)\xi]^2},$$

the variable ξ is defined implicitly as solution of the nonlinear algebraic equation[3]

$$\mathcal{E}_\xi(\xi; I_4^H, I_5^H) := 2\mathcal{S}_{\mathtt{p}}'(\mathcal{I}_5) - \xi = 0, \tag{22}$$

and $\Psi_{\mathtt{m}}$ and $\mathcal{S}_{\mathtt{p}}$ are arbitrary functions of choice (sufficiently well-behaved as elaborated below) that characterize, respectively, the elasticity and magnetization saturation of the underlying elastomeric matrix and iron particles making up the MRE. It is plain from its definition (22) that the variable ξ depends not only on the magnetic properties and volume fraction of iron particles, but also on the magnetomechanical loading.

Precisely, the homogenization solution (21) corresponds to an MRE wherein the underlying elastomeric matrix is characterized by the isotropic, incompressible, and impermeable free-energy function

$$W_{\mathtt{m}}^H(\mathbf{F},\mathbf{H}) = \begin{cases} \Psi_{\mathtt{m}}(I_1) - \dfrac{\mu_0}{2} I_5^H & \text{if} \quad J=1 \\ +\infty & \text{otherwise} \end{cases}, \tag{23}$$

while the underlying iron particles are characterized by the mechanically rigid free-energy function

$$W_{\mathtt{p}}^H(\mathbf{F},\mathbf{H}) = \begin{cases} -\mathcal{S}_{\mathtt{p}}(I_5^H) & \text{if} \quad \mathbf{F}=\mathbf{Q}\in Orth^+ \\ +\infty & \text{otherwise} \end{cases}. \tag{24}$$

Basic physical considerations dictate that the functions $\Psi_{\mathtt{m}}$ and $\mathcal{S}_{\mathtt{p}}$ satisfy the linearization conditions

$$\Psi_{\mathtt{m}}(3) = 0, \qquad \Psi_{\mathtt{m}}'(3) = \frac{G_{\mathtt{m}}}{2}, \qquad \mathcal{S}_{\mathtt{p}}(0) = 0, \qquad \mathcal{S}_{\mathtt{p}}'(0) = \frac{\mu_{\mathtt{p}}}{2}, \tag{25}$$

where $G_{\mathtt{m}} > 0$ and $\mu_{\mathtt{p}} \geq \mu_0$ denote the initial shear modulus of the elastomeric matrix and the initial permeability of the iron particles. In addition, the magnetization saturation function is required to satisfy the convexity conditions

$$\mathcal{S}_{\mathtt{p}}'(I_5^H) > 0, \qquad \mathcal{S}_{\mathtt{p}}'(I_5^H) + 2I_5^H\mathcal{S}_{\mathtt{p}}''(I_5^H) > 0, \tag{26}$$

and the growth condition

$$\mathcal{S}_{\mathtt{p}}'(I_5^H) = \frac{\mu_0}{2} + \frac{\mu_0 m_{\mathtt{p}}^s}{2\sqrt{I_5^H}} + o\left(\frac{1}{\sqrt{I_5^H}}\right) \tag{27}$$

in the limit as $I_5^H \to \infty$, where $m_{\mathtt{p}}^s \geq 0$ stands for the magnetization saturation of the iron particles.

Examples for the function $\Psi_{\mathtt{m}}$ include, for instance, the Neo-Hookean model (Treloar, 1943)

$$\Psi_{\mathtt{m}}(I_1) = \frac{G_{\mathtt{m}}}{2}\left[I_1 - 3\right], \tag{28}$$

the Lopez-Pamies (2010b) model

$$\Psi_{\mathtt{m}}(I_1) = \frac{3^{1-\alpha_1}}{2\alpha_1} G_1\left[I_1^{\alpha_1} - 3^{\alpha_1}\right] + \frac{3^{1-\alpha_2}}{2\alpha_2} G_2\left[I_1^{\alpha_2} - 3^{\alpha_2}\right], \tag{29}$$

as well as the Arruda and Boyce (1993) and Gent (1996) models among others. In this last expression, $G_1 > 0$, $G_2 \geq 0$, α_1, α_2 are real-valued material parameters, the first two of which satisfy the condition $G_1 + G_2 = G_{\mathtt{m}}$. Examples for the function $\mathcal{S}_{\mathtt{p}}$ include, for instance, the Langevin model

$$\mathcal{S}_{\mathtt{p}}(I_5^H) = \frac{\mu_0}{2} I_5^H + \frac{\mu_0 (m_{\mathtt{p}}^s)^2}{3\chi_{\mathtt{p}}}\left\{ \ln\left[\sinh\left(\frac{3\chi_{\mathtt{p}}}{m_{\mathtt{p}}^s}\sqrt{I_5^H}\right)\right] - \ln\left[\frac{3\chi_{\mathtt{p}}}{m_{\mathtt{p}}^s}\sqrt{I_5^H}\right]\right\}, \tag{30}$$

[3]Throughout, we make use of the standard convention $g'(z) = \mathrm{d}g(z)/\mathrm{d}z$ to denote the derivative of functions of a single scalar variable.

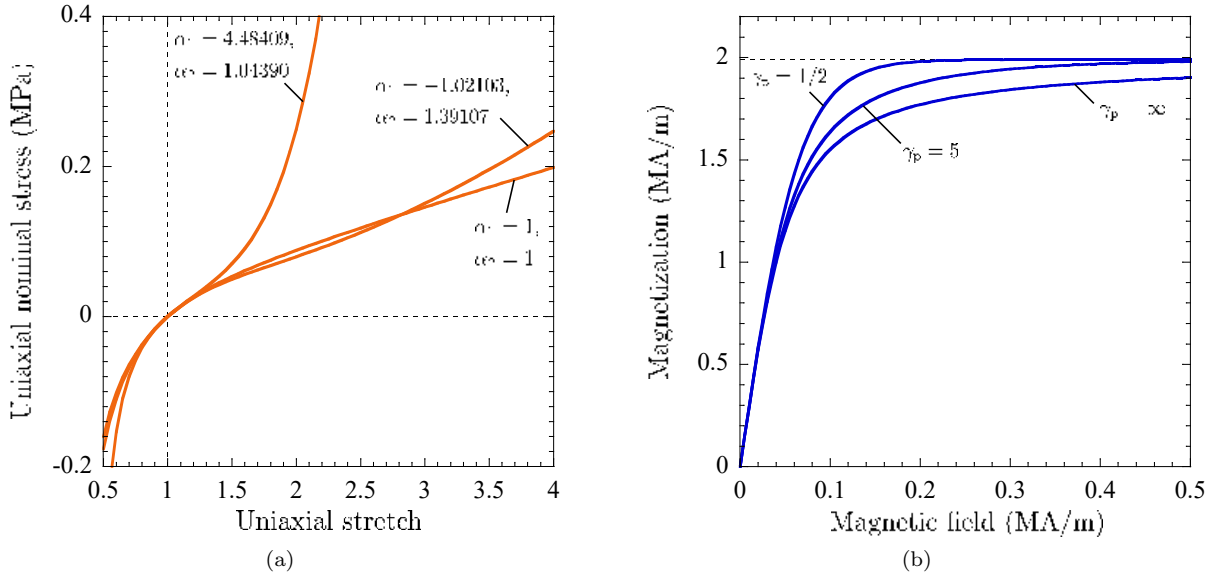

(a) (b)

Figure 1: (a) Uniaxial nominal stress-stretch curves for silicone elastomers characterized by (29) with $G_1 = 18.57$ kPa, $G_2 = 31.92$ kPa, and three different sets of values of the material parameters α_1 and α_2. (b) Uniaxial magnetization curves for iron particles characterized by (30) with $\chi_p = 30$, $\mu_0 m_p^s$=2.5 T, and three different values of the material parameter γ_p.

the Brillouin model

$$\mathcal{S}_p(I_5^H) = \frac{\mu_0}{2} I_5^H + \frac{\mu_0 m_p^{s\,2}(1+\gamma_p)}{3\gamma_p \chi_p} \left\{ \ln\left[\sinh\left(\frac{3(1+2\gamma_p)\chi_p}{2(1+\gamma_p)m_p^s}\sqrt{I_5^H}\right)\right] - \ln\left[(1+2\gamma_p)\sinh\left(\frac{3\chi_p}{2(1+\gamma_p)m_p^s}\sqrt{I_5^H}\right)\right]\right\}, \tag{31}$$

as well as many others; see, e.g., Chapter 11 in the monograph by Kittel (2004). In these last expressions, $\chi_p = \mu_p/\mu_0 - 1$ denotes the magnetic susceptibility of the iron particles and γ_p is a positive parameter of choice.

For illustration purposes, Fig. 1(a) shows uniaxial nominal stress-stretch curves implied by the Lopez-Pamies (2010b) model (29) for values of the material parameters $G_1 = 18.57$ kPa, $G_2 = 31.92$ kPa, and three different sets of values of the pair (α_1, α_2), which are descriptive of silicone elastomers (Poulain et al., 2017). Similarly, Fig. 1(b) shows uniaxial magnetization curves implied by the Brillouin model (31) for values of the material parameters $\chi_p = 30$, $\mu_0 m_p^s$=2.5 T, and three different values of γ_p, which are descriptive of standard iron particles (Psarra et al., 2017). It is of note that when $\gamma_p = 1/2$, the Brillouin model (31) reduces to the standard hyperbolic tangent model and when $\gamma_p = \infty$ it reduces to the Langevin model (30).

The following features of the solution (21) will prove useful in the sequel:

1. The constitutive relations (2) implied by the free-energy function (21) are given by

$$\begin{aligned} \mathbf{S} &= \frac{2}{(1-c)^{5/2}}\Psi_m'(\mathcal{I}_1)\mathbf{F} + \omega(\xi)\,\mathbf{F}^{-T}\mathbf{H}\otimes\mathbf{F}^{-1}\mathbf{F}^{-T}\mathbf{H} - p\mathbf{F}^{-T}, \\ \mathbf{B} &= (\nu(\xi) - \omega(\xi))\,\mathbf{H} + \omega(\xi)\,\mathbf{F}^{-1}\mathbf{F}^{-T}\mathbf{H} \end{aligned} \tag{32}$$

with p indicating the arbitrary hydrostatic pressure that arises from the incompressibility constraint $J = 1$.

In turn, the total Cauchy stress $(7)_1$, Eulerian magnetic induction $(7)_3$, and magnetization (8) are

given by

$$\begin{aligned}\boldsymbol{\sigma} &= \frac{2}{(1-c)^{5/2}}\Psi_{\mathtt{m}}'(\mathcal{I}_1)\mathbf{F}\mathbf{F}^T + \omega\left(\xi\right)\mathbf{F}^{-T}\mathbf{H}\otimes\mathbf{F}^{-T}\mathbf{H} - p\mathbf{I},\\ \mathbf{b} &= \left(\nu\left(\xi\right)-\omega\left(\xi\right)\right)\mathbf{F}\mathbf{H} + \omega\left(\xi\right)\mathbf{F}^{-T}\mathbf{H},\\ \mathbf{m} &= \frac{\nu\left(\xi\right)-\omega\left(\xi\right)}{\mu_0}\mathbf{F}\mathbf{H} + \frac{\omega\left(\xi\right)-\mu_0}{\mu_0}\mathbf{F}^{-T}\mathbf{H}.\end{aligned} \tag{33}$$

2. In the limit of small magnetic fields as[4] $|\mathbf{H}|\to 0$, the nonlinear algebraic equation (22) admits the explicit asymptotic solution $\xi = \mu_{\mathtt{p}} + O(|\mathbf{H}|^2)$; note that in such a limit $\mathcal{I}_5 = O(|\mathbf{H}|^2)$. It follows, in turn, that the finite branch of the free-energy function (21) reduces asymptotically to the fully explicit expression

$$W^H(I_1, I_4^H, I_5^H) = (1-c)\Psi_{\mathtt{m}}\left(\mathcal{I}_1\right) + \frac{1}{2}\left[\omega\left(\mu_{\mathtt{p}}\right) - \nu\left(\mu_{\mathtt{p}}\right)\right]I_4^H - \frac{\omega\left(\mu_{\mathtt{p}}\right)}{2}I_5^H + O\left(|\mathbf{H}|^3\right). \tag{34}$$

In the absence of deformation when $\mathbf{F}=\mathbf{I}$, it immediately follows from (34) that the solution (21) implies the results

$$\mu = \nu(\mu_{\mathtt{p}}) = \mu_0 + \frac{3c\mu_0(\mu_{\mathtt{p}}-\mu_0)}{[(2+c)\mu_0 + (1-c)\mu_{\mathtt{p}}]} \qquad \text{and} \qquad \chi = \frac{\mu}{\mu_0} - 1 \tag{35}$$

for the initial permeability μ and susceptibility χ of the MRE in terms of the initial permeability $\mu_{\mathtt{p}}$ and the volume fraction c of the underlying iron particles.

In the absence of magnetic fields when $\mathbf{H}=\mathbf{0}$, the result (34) reduces to

$$W^H(I_1, 0, 0) = (1-c)\Psi_{\mathtt{m}}\left(\mathcal{I}_1\right), \tag{36}$$

which is precisely the homogenization solution derived by Lopez-Pamies et al. (2013); Leonard et al. (2020) have just provided experimental evidence of the high accuracy of the result of (36) for elastomers filled with spherical particles that are of micrometer size or larger, which is typically the case for iron particles. In the limit of small deformations as $\mathbf{F}\to\mathbf{I}$, the free-energy function (36) reduces further to

$$W^H(I_1, 0, 0) = \frac{G_{\mathtt{m}}}{(1-c)^{5/2}}\mathrm{tr}\,\boldsymbol{\varepsilon}^2 + O\left(\|\boldsymbol{\varepsilon}\|^3\right), \tag{37}$$

where $\boldsymbol{\varepsilon} = (\mathbf{F}+\mathbf{F}^T-2\mathbf{I})/2$ stands for the infinitesimal strain tensor. It immediately follows from (37) that the solution (21) implies the result

$$G = \frac{G_{\mathtt{m}}}{(1-c)^{5/2}} \tag{38}$$

for the initial shear modulus G of the MRE in terms of the initial shear modulus $G_{\mathtt{m}}$ of the underlying elastomeric matrix and the volume fraction c of iron particles.

3. In the limit of large magnetic fields as $|\mathbf{H}|\to\infty$, the nonlinear algebraic equation (22) admits the explicit asymptotic solution $\xi = \mu_0 + \mu_0 m_{\mathtt{p}}^s/\sqrt{I_5^H} + o(|\mathbf{H}|^{-1})$, from which it follows that $\mathcal{I}_5 = I_5^H + O(|\mathbf{H}|)$, $\nu(\xi) = \omega(\xi) = \mu_0 + c\,m_{\mathtt{p}}^s\mu_0/\sqrt{I_5^H} + o(|\mathbf{H}|^{-1})$, and hence that the free-energy function (21) reduces asymptotically to the fully explicit expression

$$W^H(I_1, I_4^H, I_5^H) = (1-c)\Psi_{\mathtt{m}}\left(\mathcal{I}_1\right) + c(1-c)\mu_0(m_{\mathtt{p}}^s)^2\left[\frac{1}{6} + \frac{c}{10}\left(\frac{I_4^H}{I_5^H}-1\right)\right] - c\,\mu_0 m_{\mathtt{p}}^s\sqrt{I_5^H} - \frac{\mu_0}{2}I_5^H + O\left(|\mathbf{H}|^{-1}\right). \tag{39}$$

[4]Here and subsequently, the notation $|\cdot|$ is used to denote the Euclidian norm $||\cdot||_2$.

In turn, it follows that the magnetization (33) reduces asymptotically to leading order to

$$\mathbf{m} = m\frac{\mathbf{F}^{-T}\mathbf{H}}{|\mathbf{F}^{-T}\mathbf{H}|} = m^s\frac{\mathbf{h}}{|\mathbf{h}|} \qquad \text{with} \qquad m^s = c\,m_{\mathrm{p}}^s, \tag{40}$$

which readily identifies m^s as the magnetization saturation of the MRE. That is, the magnetization saturation of the MRE is nothing more than the arithmetic mean of the magnetization saturation of the elastomer $m_{\mathrm{m}}^s = 0$ and of the iron particles m_{p}^s: $m^s = (1-c)m_{\mathrm{m}}^s + c\,m_{\mathrm{p}}^s = c\,m_{\mathrm{p}}^s$.

4. For arbitrary magnetic fields $\mathbf{H}$ that are neither small nor large in magnitude, the nonlinear algebraic equation (22) defining the variable ξ needs to be solved numerically. Equation (22) happens to be a fixed-point equation of the form

$$g(\xi) = \xi \qquad \text{with} \qquad g(\xi) := 2\mathcal{S}_{\mathrm{p}}'(\mathcal{I}_5). \tag{41}$$

Provided that (41) satisfies the Banach-Caccioppoli fixed-point theorem, it then follows that its solution can be simply written as the limit of a *fully explicit* fixed-point iteration. Precisely,

$$\xi = \lim_{r\to\infty} \xi_{r+1} \quad \text{where} \quad \xi_{r+1} = g(\xi_r) \quad \text{with initial term} \quad \xi_0 = \mu_0. \tag{42}$$

By way of an example, when the magnetization saturation function $\mathcal{S}_{\mathrm{p}}$ is given by the Langevin model (30), numerical tests indicate that just 20 iterations in the iteration scheme (42) are sufficient to generate accurate solutions for ξ, this for any volume of fraction of the iron particles c, any values of their permeability μ_{p} and magnetization saturation m_{p}^s, and any values of the invariants I_4^H and I_5^H. Alternatively, it is also a simple matter to solve equation (22) by means of a conventional Newton-Raphson scheme.

4. A family of explicit free-energy functions $W^H(\mathbf{F},\mathbf{H})$ for MREs containing iron particles

Having recalled the homogenization solution (21) of Lefèvre et al. (2017) for MREs containing iron particles and having spelled out its relevant features for the purposes of this paper, we now proceed with the construction of a family of fully explicit free-energy functions W^H as approximations of (21). The construction adheres to the following three-fold guiding principle:

- the proposed explicit free energies are given by the formula (21) where the variable ξ defined *implicitly* by equation (22) is replaced by an *explicit* approximate expression such that the resulting free-energy functions
- agree identically with the homogenization solution (34) in the limit of small magnetic fields as $|\mathbf{H}| \to 0$, this for arbitrary finite deformation gradients $\mathbf{F}$,
- and with the homogenization solution (39) in the limit of large magnetic fields as $|\mathbf{H}| \to \infty$, this for arbitrary finite deformation gradients $\mathbf{F}$.

The above two asymptotic requirements in the limits of small and large magnetic fields are readily satisfied by any choice of ξ such that

$$\xi = \mu_{\mathrm{p}} + O\left(|\mathbf{H}|^p\right) \quad p > 0 \quad \text{in the limit as} \quad |\mathbf{H}| \to 0$$

and

$$\xi = \mu_0 + \frac{\mu_0\, m_{\mathrm{p}}^s}{\sqrt{I_5^H}} + O\left(|\mathbf{H}|^{-q}\right) \quad q > 1 \quad \text{in the limit as} \quad |\mathbf{H}| \to \infty.$$

A relatively simple choice of ξ that is consistent with these asymptotic requirements and that in addition, as elaborated in Section 7 below, leads to explicit free-energy functions W^H in close agreement with (21) for arbitrary deformation gradients $\mathbf{F}$ and magnetic fields $\mathbf{H}$ is given by

$$\xi = \mu_{\mathtt{p}} - \frac{a_0 I_5^H + a_1 (I_5^H)^{3/2} + a_2 (I_5^H)^2}{a_3 + a_4 (I_5^H)^{1/2} + a_5 I_5^H + a_6 (I_5^H)^{3/2} + a_7 (I_5^H)^2}, \tag{43}$$

where

$$\begin{aligned}
a_0 =& \frac{27(\mu_{\mathtt{p}} - \mu_0)^3 a_3}{5(m_{\mathtt{p}}^s)^2[(2+c)\mu_0 + (1-c)\mu_{\mathtt{p}}]^2}, \quad a_1 = \frac{27(\mu_{\mathtt{p}} - \mu_0)^3 a_4}{5(m_{\mathtt{p}}^s)^2[(2+c)\mu_0 + (1-c)\mu_{\mathtt{p}}]^2}, \quad a_2 = (\mu_{\mathtt{p}} - \mu_0) a_7, \\
a_3 =& 5(m_{\mathtt{p}}^s)^4 \mu_0 [(2+c)\mu_0 + (1-c)\mu_{\mathtt{p}}]^2 \left[\left(5c^5 + 20c^4 + 39c^3 + 49c^2 + 40c + 9\right) \mu_0^5 + \right. \\
& (1-c)\left(25c^4 + 80c^3 + 117c^2 + 98c + 40\right) \mu_0^4 \mu_{\mathtt{p}} + (1-c)^2 \left(50c^3 + 120c^2 + 117c + 49\right) \mu_0^3 \mu_{\mathtt{p}}^2 + \\
& \left. (1-c)^3 \left(50c^2 + 80c + 39\right) \mu_0^2 \mu_{\mathtt{p}}^3 + 5(1-c)^4 (5c+4) \mu_0 \mu_{\mathtt{p}}^4 + 5(1-c)^5 \mu_{\mathtt{p}}^5 \right], \\
a_4 =& 15(m_{\mathtt{p}}^s)^3 \mu_0 (\mu_{\mathtt{p}} - \mu_0) [(2+c)\mu_0 + (1-c)\mu_{\mathtt{p}}]^2 \left[\left(5c^4 + 25c^3 + 27c^2 + 40c + 11\right) \mu_0^4 + \right. \\
& \left. (1-c)\left(20c^3 + 75c^2 + 54c + 40\right) \mu_0^3 \mu_{\mathtt{p}} + 3(1-c)^2 \left(10c^2 + 25c + 9\right) \mu_0^2 \mu_{\mathtt{p}}^2 + 5(1-c)^3 (4c+5) \mu_0 \mu_{\mathtt{p}}^3 + 5(1-c)^4 \mu_{\mathtt{p}}^4 \right], \\
a_5 =& 9(m_{\mathtt{p}}^s)^2 \mu_0 (\mu_{\mathtt{p}} - \mu_0)^2 \left[\left(40c^5 + 240c^4 + 602c^3 + 701c^2 + 681c + 166\right) \mu_0^5 + \right. \\
& (1-c)\left(200c^4 + 960c^3 + 1806c^2 + 1402c + 681\right) \mu_0^4 \mu_{\mathtt{p}} + (1-c)^2 \left(400c^3 + 1440c^2 + 1806c + 701\right) \mu_0^3 \mu_{\mathtt{p}}^2 + \\
& \left. 2(1-c)^3 \left(200c^2 + 480c + 301\right) \mu_0^2 \mu_{\mathtt{p}}^3 + 40(1-c)^4 (5c+6) \mu_0 \mu_{\mathtt{p}}^4 + 40(1-c)^5 \mu_{\mathtt{p}}^5 \right], \\
a_6 =& 27 m_{\mathtt{p}}^s \mu_0 (\mu_{\mathtt{p}} - \mu_0)^3 \left[\left(40c^4 + 185c^3 + 231c^2 + 281c + 73\right) \mu_0^4 + (1-c)\left(160c^3 + 555c^2 + 462c + 281\right) \mu_0^3 \mu_{\mathtt{p}} + \right. \\
& \left. 3(1-c)^2 \left(80c^2 + 185c + 77\right) \mu_0^2 \mu_{\mathtt{p}}^2 + 5(1-c)^3 (32c+37) \mu_0 \mu_{\mathtt{p}}^3 + 40(1-c)^4 \mu_{\mathtt{p}}^4 \right], \\
a_7 =& 27(\mu_{\mathtt{p}} - \mu_0)^4 \left[\left(5c^2 + 5c + 8\right) \left(5c^2 + 17c + 5\right) \mu_0^4 + (1-c)(10c+23) \left(10c^2 + 10c + 7\right) \mu_0^3 \mu_{\mathtt{p}} + \right. \\
& \left. 30(1-c)^2 \left(5c^2 + 11c + 5\right) \mu_0^2 \mu_{\mathtt{p}}^2 + 10(1-c)^3 (10c+11) \mu_0 \mu_{\mathtt{p}}^3 + 25(1-c)^4 \mu_{\mathtt{p}}^4 \right].
\end{aligned} \tag{44}$$

Guided by the full numerical solution of (22) for ξ, the approximate expression (43) was constructed by interpolating with a rational function the asymptotically exact solution for ξ when $I_4^H = I_5^H$ up to orders $O\left((I_5^H)^2\right)$ and $O\left((I_5^H)^{-5/2}\right)$ for the basic choice of the Langevin function (30) for the function $\mathcal{S}_{\mathtt{p}}$.

Making use of the variable (43) — instead of that defined implicitly by equation (22) — in (21) leads to the proposed family of fully explicit free-energy functions:

$$W^H(\mathbf{F}, \mathbf{H}) = \begin{cases} W^H(I_1, I_4^H, I_5^H) = W_{mech}(I_1) + W_{mag}^H(I_5^H) + W_{couple}^H(I_4^H, I_5^H) - \dfrac{\mu_0}{2} I_5^H & \text{if} \quad J = 1 \\ +\infty & \text{otherwise} \end{cases} \tag{45}$$

with

$$\begin{aligned}
W_{mech}(I_1) &= (1-c)\Psi_{\mathtt{m}}\left(\frac{I_1 - 3}{(1-c)^{7/2}} + 3\right), \\
W_{mag}^H(I_5^H) &= -\frac{1}{2}\left(\frac{3c(10 + 2c + 3c^2)(\xi - \mu_0)\mu_0^2}{5[(2+c)\mu_0 + (1-c)\xi]^2} + \frac{3c(1-c)(5+3c)(\xi - \mu_0)\mu_0 \xi}{5[(2+c)\mu_0 + (1-c)\xi]^2}\right) I_5^H, \\
W_{couple}^H(I_4^H, I_5^H) &= -c\,\mathcal{S}_{\mathtt{p}}(\mathcal{I}_5) + \frac{c\,\xi}{2}\mathcal{I}_5 + \frac{1}{2}(\omega(\xi) - \nu(\xi)) I_4^H,
\end{aligned}$$

where we recall that

$$\begin{aligned}
\mathcal{I}_5 &= -\frac{54c(1-c)(\xi - \mu_0)\mu_0^2}{5[(2+c)\mu_0 + (1-c)\xi]^3} I_4^H + \frac{9[(10 - c + 6c^2)\mu_0 + (5 + c - 6c^2)\xi]\mu_0^2}{5[(2+c)\mu_0 + (1-c)\xi]^3} I_5^H, \\
\nu(\xi) &= \mu_0 + \frac{3c\mu_0(\xi - \mu_0)}{[(2+c)\mu_0 + (1-c)\xi]}, \\
\omega(\xi) &= \mu_0 + \frac{3c(10 + 2c + 3c^2)(\xi - \mu_0)\mu_0^2}{5[(2+c)\mu_0 + (1-c)\xi]^2} + \frac{3c(1-c)(5+3c)(\xi - \mu_0)\mu_0 \xi}{5[(2+c)\mu_0 + (1-c)\xi]^2}.
\end{aligned}$$

Remark 6. *The two material functions and three material parameters in (45) and their calibration.* The free-energy function (45) contains two material functions, $\Psi_{\mathtt{m}}(I_1)$ and $\mathcal{S}_{\mathtt{p}}(I_5^H)$ subject to the conditions (25)–(27), and three material parameters, $\mu_{\mathtt{p}} \geq \mu_0$, $m_{\mathtt{p}}^s \geq 0$, and $c \in [0,1]$. Physically, again, the function $\Psi_{\mathtt{m}}(I_1)$ describes the elastic response of the elastomeric matrix in the MRE. The function $\mathcal{S}_{\mathtt{p}}(I_5^H)$ describes the magnetization of the iron particles in the MRE, with $\mu_{\mathtt{p}}$ and $m_{\mathtt{p}}^s$ describing their initial permeability and magnetization saturation, while c corresponds to their volume fraction.

For cases when all these five inputs are known from the fabrication process of the MRE of interest, no calibration of (45) is needed. On the other hand, for cases when none (or only some) of these inputs are known, one would have to make use of specific functional forms for $\Psi_{\mathtt{m}}(I_1)$ and $\mathcal{S}_{\mathtt{p}}(I_5^H)$, and then fit their material parameters together with $\mu_{\mathtt{p}}$, $m_{\mathtt{p}}^s$, and c to experimental data on the MRE.

By way of an example, consider a case when no information about the fabrication process of an MRE of interest is available, save that it is made of an elastomer isotropically filled with equiaxed iron particles. Choosing the Lopez-Pamies (29) and Brillouin (31) models for the material functions $\Psi_{\mathtt{m}}(I_1)$ and $\mathcal{S}_{\mathtt{p}}(I_5^H)$ would result in a free-energy function (45) with eight material parameters: G_1, G_2, α_1, α_2, $\mu_{\mathtt{p}}$, $m_{\mathtt{p}}^s$, $\gamma_{\mathtt{p}}$, and c. The first four of these, together with the volume fraction of the iron particles, control the mechanical response of the MRE at small, intermediate, and large deformations. Accordingly, they could be easily calibrated by fitting a uniaxial tension test in the absence of magnetic fields; see, e.g., Section 5 in Meddeb et al. (2019). The remaining three parameters, also together with the volume fraction of the iron particles, control the magnetic response of the MRE at small, intermediate, and large magnetic fields. Accordingly, they could be easily calibrated by fitting a uniaxial magnetization test; see, e.g., Chapter 2 in Diguet (2010) and Section 2.2 in Danas et al. (2012).

Remark 7. *The limits when $c = 0$ and $c = 1$.* In the absence of iron particles when $c = 0$, the free-energy function (45) reduces to that of the elastomer, namely,

$$W^H(\mathbf{F},\mathbf{H}) = \begin{cases} \Psi_{\mathtt{m}}(I_1) - \dfrac{\mu_0}{2} I_5^H & \text{if} \quad J = 1 \\ +\infty & \text{otherwise} \end{cases}.$$

Similarly, when $c = 1$ the free-energy function (45) reduces to that of the iron particles:

$$W^H(\mathbf{F},\mathbf{H}) = \begin{cases} -\mathcal{S}_{\mathtt{p}}(I_5^H) & \text{if} \quad \mathbf{F} = \mathbf{Q} \in Orth^+ \\ +\infty & \text{otherwise} \end{cases}.$$

Remark 8. *The constitutive relations (2).* The constitutive relations (2) implied by the free-energy function (45) are given by

$$\begin{aligned} \mathbf{S} &= \frac{2}{(1-c)^{5/2}} \Psi_{\mathtt{m}}' \left(\frac{I_1 - 3}{(1-c)^{7/2}} + 3 \right) \mathbf{F} + \left[\omega(\xi) + c \left(2\mathcal{S}_{\mathtt{p}}'(\mathcal{I}_5) - \xi \right) \frac{\partial \mathcal{I}_5}{\partial I_5^H} \right] \mathbf{F}^{-T}\mathbf{H} \otimes \mathbf{F}^{-1}\mathbf{F}^{-T}\mathbf{H} - p\mathbf{F}^{-T}, \\ \mathbf{B} &= \left[\nu(\xi) - \omega(\xi) + c \left(2\mathcal{S}_{\mathtt{p}}'(\mathcal{I}_5) - \xi \right) \frac{\partial \mathcal{I}_5}{\partial I_4^H} \right] \mathbf{H} + \left[\omega(\xi) + c \left(2\mathcal{S}_{\mathtt{p}}'(\mathcal{I}_5) - \xi \right) \frac{\partial \mathcal{I}_5}{\partial I_5^H} \right] \mathbf{F}^{-1}\mathbf{F}^{-T}\mathbf{H}, \end{aligned} \tag{46}$$

where the derivatives $\partial \mathcal{I}_5 / \partial I_4^H$ and $\partial \mathcal{I}_5 / \partial I_5^H$ are spelled out in Appendix A.1 and where p stands for an arbitrary hydrostatic pressure.

Remark 9. *The corresponding $(\mathbf{F},\mathbf{B})$ version.* For typical choices of magnetization saturation function $\mathcal{S}_{\mathtt{p}}(I_5^H)$, such as (30) or (31) with a finite value of magnetization saturation $m_{\mathtt{p}}^s$, the free-energy function (45) does not admit an explicit partial inversion of $\mathbf{H}$ in favor of $\mathbf{B}$. It is thus not possible in general to generate a corresponding free energy W^B that is fully explicit. One notable exception is the case when the magnetic behavior of the iron particles is idealized as linear (i.e., when $m_{\mathtt{p}}^s = \infty$). For such a case, the partial Legendre transform (5) of the free-energy function (45) can be shown to be given by the fully explicit

expression

$$W^B(\mathbf{F},\mathbf{B}) = (1-c)\Psi_{\mathtt{m}}\left(\frac{I_1-3}{(1-c)^{7/2}}+3\right)+\frac{1}{2\omega(\mu_{\mathtt{p}})}\left[\frac{I_5^B+\eta^2 I_4^B+\eta\left(I_1 I_5^B-I_6^B\right)}{1+\eta^3+\eta^2 I_2+\eta I_1}\right],$$

where $\eta = (\nu(\mu_{\mathtt{p}})-\omega(\mu_{\mathtt{p}}))/\omega(\mu_{\mathtt{p}})$ and where we recall that the invariants I_2 and I_4^B, I_5^B, I_6^B are given by $(10)_2$ and (12) in terms of the deformation gradient $\mathbf{F}$ and the Lagrangian magnetic induction $\mathbf{B}$. Making use of this last result, it is possible to generate fully explicit free-energy functions W^B for arbitrary choices of the magnetization saturation function $\mathcal{S}_{\mathtt{p}}(I_5^H)$ by approximating the homogenization solution (47) directly in the $(\mathbf{F},\mathbf{B})$ domain. An example of such an approximation is given in Section of 4.2.2 of Mukherjee et al. (2020).

5. The homogenization solution of Lefèvre et al. (2017) for MREs containing ferrofluid particles

For the case of MREs comprised of an isotropic incompressible elastomer filled with a random isotropic distribution of spherical ferrofluid particles, the solution of Lefèvre et al. (2017) reads as

$$W^H(\mathbf{F},\mathbf{H}) = \begin{cases} W^H(I_1,I_4^H,I_5^H) = (1-c)\Psi_{\mathtt{m}}\left(\mathcal{J}_1\right) - c\,\mathcal{S}_{\mathtt{p}}\left(\mathcal{J}_5\right) + \dfrac{c\,\zeta}{2}\mathcal{J}_5 + \dfrac{1}{2}\left(w\left(\zeta\right)-v\left(\zeta\right)\right)I_4^H - \dfrac{w\left(\zeta\right)}{2}I_5^H & \text{if} \quad J=1 \\ +\infty & \text{otherwise} \end{cases}, \tag{47}$$

where $c\in[0,1]$ denotes the volume fraction of ferrofluid particles,

$$\begin{aligned}
\mathcal{J}_1 &= (1-c)^{2/3}\left(I_1-3\right)+3, \\
\mathcal{J}_5 &= \frac{3(1500-1900c+729c^{36/25})(\zeta-\mu_0)\mu_0^2}{250[(2+c)\mu_0+(1-c)\zeta]^3}I_4^H - \frac{3[(750-1150c+729c^{36/25})(\zeta-\mu_0)-2250\mu_0]\mu_0^2}{250[(2+c)\mu_0+(1-c)\zeta]^3}I_5^H, \\
v\left(\zeta\right) &= \mu_0 + \frac{3c\mu_0(\zeta-\mu_0)}{(2+c)\mu_0+(1-c)\zeta}, \\
w\left(\zeta\right) &= \mu_0 + \frac{9c^2(\zeta-\mu_0)^2\mu_0}{[(2+c)\mu_0+(1-c)\zeta]^2}\left[\frac{4}{45}-\frac{81c^{11/25}}{500}+\frac{\mu_0}{c(\zeta-\mu_0)}\right],
\end{aligned}$$

the variable ζ is defined implicitly as solution of the nonlinear algebraic equation

$$\mathcal{E}_\zeta(\zeta;I_4^H,I_5^H) := 2\mathcal{S}_{\mathtt{p}}'\left(\mathcal{J}_5\right)-\zeta = 0, \tag{48}$$

and where, as in the preceding sections, $\Psi_{\mathtt{m}}$ and $\mathcal{S}_{\mathtt{p}}$ are arbitrary functions of choice, subject to the conditions (25)–(27), that physically characterize the elasticity and magnetization saturation of the underlying elastomeric matrix and ferrofluid particles making up the MRE. It is plain from its definition (48) that the variable ζ depends not only on the magnetic properties and volume fraction of ferrofluid particles, but also on the magnetomechanical loading.

Precisely, the homogenization solution (47) corresponds to an MRE wherein the underlying elastomeric matrix, much like that for the solution (21), is characterized by the isotropic, incompressible, and impermeable free-energy function (23), while the underlying ferrofluid particles are characterized by the free-energy function

$$W_{\mathtt{p}}^H(\mathbf{F},\mathbf{H}) = \begin{cases} -\mathcal{S}_{\mathtt{p}}(I_5^H) & \text{if} \quad J=1 \\ +\infty & \text{otherwise} \end{cases}. \tag{49}$$

Note that this free-energy function describes the mechanical behavior of the ferrofluid particles as an incompressible elastic fluid; see, e.g., Section 4.2.4 in the monograph by Ogden (1997). That is, no energy is

needed to change their shape but an infinite energy would be required to change their volume. The function $\mathcal{S}_{\mathtt{p}}(I_5^H)$ in (49), much like in the free-energy function (24) characterizing iron particles, allows to describe a truly wide range of magnetic behaviors for the ferrofluid particles.

For use in the next section, we record now a number of features of the solution (47):

1. The constitutive relations (2) implied by the free-energy function (47) are given by

$$\begin{aligned}\mathbf{S} &= 2(1-c)^{5/3}\Psi_{\mathtt{m}}'(\mathcal{J}_1)\mathbf{F} + w\left(\zeta\right)\mathbf{F}^{-T}\mathbf{H}\otimes\mathbf{F}^{-1}\mathbf{F}^{-T}\mathbf{H} - p\mathbf{F}^{-T},\\ \mathbf{B} &= \left(v\left(\zeta\right)-w\left(\zeta\right)\right)\mathbf{H} + w\left(\zeta\right)\mathbf{F}^{-1}\mathbf{F}^{-T}\mathbf{H},\end{aligned} \tag{50}$$

   where p again stands for an arbitrary hydrostatic pressure.

   It follows that the total Cauchy stress $(7)_1$, Eulerian magnetic induction $(7)_3$, and magnetization (8) are given in turn by

$$\begin{aligned}\boldsymbol{\sigma} &= 2(1-c)^{5/3}\Psi_{\mathtt{m}}'(\mathcal{J}_1)\mathbf{F}\mathbf{F}^T + w\left(\zeta\right)\mathbf{F}^{-T}\mathbf{H}\otimes\mathbf{F}^{-T}\mathbf{H} - p\mathbf{I},\\ \mathbf{b} &= \left(v\left(\zeta\right)-w\left(\zeta\right)\right)\mathbf{F}\mathbf{H} + w\left(\zeta\right)\mathbf{F}^{-T}\mathbf{H},\\ \mathbf{m} &= \frac{v\left(\zeta\right)-w\left(\zeta\right)}{\mu_0}\mathbf{F}\mathbf{H} + \frac{w\left(\zeta\right)-\mu_0}{\mu_0}\mathbf{F}^{-T}\mathbf{H}.\end{aligned} \tag{51}$$

2. In the limit of small magnetic fields as $|\mathbf{H}|\to 0$, the nonlinear algebraic equation (48) admits the explicit asymptotic solution $\zeta = \mu_{\mathtt{p}} + O(|\mathbf{H}|^2)$; note that in such a limit $\mathcal{I}_5 = O(|\mathbf{H}|^2)$. With this, one can easily deduce that the finite branch of the free-energy function (47) reduces asymptotically to the fully explicit expression

$$W^H(I_1, I_4^H, I_5^H) = (1-c)\Psi_{\mathtt{m}}\left(\mathcal{J}_1\right) + \frac{1}{2}\left[w\left(\mu_{\mathtt{p}}\right) - v\left(\mu_{\mathtt{p}}\right)\right]I_4^H - \frac{w\left(\mu_{\mathtt{p}}\right)}{2}I_5^H + O\left(|\mathbf{H}|^3\right) \tag{52}$$

   as $|\mathbf{H}|\to 0$.

   In the absence of deformation when $\mathbf{F}=\mathbf{I}$, it follows from (52) that the solution (47) implies the results

$$\mu = v(\mu_{\mathtt{p}}) = \mu_0 + \frac{3c\mu_0(\mu_{\mathtt{p}}-\mu_0)}{[(2+c)\mu_0 + (1-c)\mu_{\mathtt{p}}]} \qquad \text{and} \qquad \chi = \frac{\mu}{\mu_0} - 1 \tag{53}$$

   for the initial permeability μ and susceptibility χ of the MRE in terms of the initial permeability $\mu_{\mathtt{p}}$ and the volume fraction c of the underlying ferrofluid particles. Note that (53) agree identically with the results (35) for MREs containing iron particles.

   In the absence of magnetic fields when $\mathbf{H}=\mathbf{0}$, the result (52) reduces to

$$W^H(I_1,0,0) = (1-c)\Psi_{\mathtt{m}}\left(\mathcal{J}_1\right), \tag{54}$$

   a homogenization solution originally derived in (Lefèvre and Lopez-Pamies, 2017a). In the limit of small deformations as $\mathbf{F}\to\mathbf{I}$, the free-energy function (54) reduces further to

$$W^H(I_1,0,0) = (1-c)^{5/3}G_{\mathtt{m}}\,\boldsymbol{\varepsilon}^2 + O\left(\|\boldsymbol{\varepsilon}\|^3\right), \tag{55}$$

   where we recall that $\boldsymbol{\varepsilon} = (\mathbf{F}+\mathbf{F}^T-2\mathbf{I})/2$ is the infinitesimal strain tensor. This last result makes it plain that the solution (47) implies the result

$$G = (1-c)^{5/3}G_{\mathtt{m}} \tag{56}$$

   for the initial shear modulus G of the MRE in terms of the initial shear modulus $G_{\mathtt{m}}$ of the underlying elastomeric matrix and the volume fraction c of ferrofluid particles.

3. In the limit of large magnetic fields as $|\mathbf{H}| \to \infty$, the nonlinear algebraic equation (48) admits as well an explicit asymptotic solution. That solution reads as $\zeta = \mu_0 + \mu_0 m_{\mathtt{p}}^s / \sqrt{I_5^H} + o(|\mathbf{H}|^{-1})$. With this, one can easily deduce that $\mathcal{I}_5 = I_5^H + O(|\mathbf{H}|)$, $v(\zeta) = w(\zeta) = \mu_0 + c\, m_{\mathtt{p}}^s \mu_0 / \sqrt{I_5^H} + o(|\mathbf{H}|^{-1})$, and in turn that the free-energy function (47) reduces asymptotically to the fully explicit expression

$$W^H(I_1, I_4^H, I_5^H) = (1-c)\Psi_{\mathtt{m}}(\mathcal{J}_1) + c\mu_0 (m_{\mathtt{p}}^s)^2 \left[\frac{1-c}{6} - \left(\frac{1}{6} - \frac{19c}{90} + \frac{81 c^{36/25}}{1000} \right) \left(\frac{I_4^H}{I_5^H} - 1 \right) \right] - c\,\mu_0 m_{\mathtt{p}}^s \sqrt{I_5^H} - \frac{\mu_0}{2} I_5^H + O\left(|\mathbf{H}|^{-1}\right) \tag{57}$$

as $|\mathbf{H}| \to \infty$. The corresponding magnetization (51) is then simply given by

$$\mathbf{m} = m \frac{\mathbf{F}^{-T}\mathbf{H}}{|\mathbf{F}^{-T}\mathbf{H}|} = m^s \frac{\mathbf{h}}{|\mathbf{h}|} \qquad \text{with} \qquad m^s = c\, m_{\mathtt{p}}^s \tag{58}$$

to leading order. As it was the case for MREs containing iron particles, the result (58) indicates that the magnetization saturation m^s of MREs containing ferrofluid particles is nothing more than the arithmetic mean of the magnetization saturation of the elastomer $m_{\mathtt{m}}^s = 0$ and of the ferrofluid particles $m_{\mathtt{p}}^s$.

4. For arbitrary magnetic fields $\mathbf{H}$ that are neither small nor large in magnitude, the nonlinear algebraic equation (48) defining the variable ζ needs to be solved numerically. Much like its counterpart (22) for the case of MREs containing iron particles, Equation (48) is a fixed-point equation and hence amenable to the use of a fully explicit fixed-point iteration method of solution of the type (42).

6. A family of explicit free-energy functions $W^H(\mathbf{F}, \mathbf{H})$ for MREs containing ferrofluid particles

In order to construct a family of fully explicit free-energy functions W^H that approximate the homogenization solution (47) for MREs containing ferrofluid particles, we follow the same three-fold guiding principle adopted for MREs containing iron particles:

- the proposed explicit free energies are given by the formula (47) where the variable ζ defined *implicitly* by equation (48) is replaced by an *explicit* approximate expression such that the resulting free-energy functions
- agree identically with the homogenization solution (52) in the limit of small magnetic fields as $|\mathbf{H}| \to 0$, this for arbitrary finite deformation gradients $\mathbf{F}$,
- and with the homogenization solution (57) in the limit of large magnetic fields as $|\mathbf{H}| \to \infty$, this for arbitrary finite deformation gradients $\mathbf{F}$.

Now, any choice of ζ that satisfies the asymptotic behaviors

$$\zeta = \mu_{\mathtt{p}} + O\left(|\mathbf{H}|^p\right) \quad p > 0 \quad \text{in the limit as} \quad |\mathbf{H}| \to 0$$

and

$$\zeta = \mu_0 + \frac{\mu_0\, m_{\mathtt{p}}^s}{\sqrt{I_5^H}} + O\left(|\mathbf{H}|^{-q}\right) \quad q > 1 \quad \text{in the limit as} \quad |\mathbf{H}| \to \infty$$

suffices to satisfy the two above asymptotic requirements for small and large magnetic fields $\mathbf{H}$. Here, because of its relative simplicity and accuracy, see Section 7 below, we propose the same formula as for MREs containing iron particles. In the present context, we write

$$\zeta = \mu_{\mathtt{p}} - \frac{a_0 I_5^H + a_1 (I_5^H)^{3/2} + a_2 (I_5^H)^2}{a_3 + a_4 (I_5^H)^{1/2} + a_5 I_5^H + a_6 (I_5^H)^{3/2} + a_7 (I_5^H)^2}, \tag{59}$$

where the coefficients $a_0, \ldots, a_7$ are given by (44).

Making use of the variable (59) — instead of that defined implicitly by equation (48) — in (47) leads to the proposed family of fully explicit free-energy functions:

$$W^H(\mathbf{F},\mathbf{H}) = \begin{cases} W^H(I_1, I_4^H, I_5^H) = W_{mech}(I_1) + W_{mag}^H(I_5^H) + W_{couple}^H(I_4^H, I_5^H) - \dfrac{\mu_0}{2} I_5^H & \text{if} \quad J = 1 \\ +\infty & \text{otherwise} \end{cases} \tag{60}$$

with

$$\begin{aligned} W_{mech}(I_1) &= (1-c)\Psi_{\mathtt{m}}\left((1-c)^{2/3}(I_1-3)+3\right), \\ W_{mag}^H(I_5^H) &= -\frac{9c^2(\zeta-\mu_0)^2\mu_0}{2[(2+c)\mu_0+(1-c)\zeta]^2}\left[\frac{4}{45} - \frac{81c^{11/25}}{500} + \frac{\mu_0}{c(\zeta-\mu_0)}\right] I_5^H, \\ W_{couple}^H(I_4^H, I_5^H) &= -c\,\mathcal{S}_{\mathtt{p}}(\mathcal{J}_5) + \frac{c\,\zeta}{2}\mathcal{J}_5 + \frac{1}{2}\left(w(\zeta) - v(\zeta)\right) I_4^H, \end{aligned}$$

where we recall that

$$\begin{aligned} \mathcal{J}_5 &= \frac{3(1500 - 1900c + 729c^{36/25})(\zeta-\mu_0)\mu_0^2}{250[(2+c)\mu_0+(1-c)\zeta]^3} I_4^H - \frac{3[(750 - 1150c + 729c^{36/25})(\zeta-\mu_0) - 2250\mu_0]\mu_0^2}{250[(2+c)\mu_0+(1-c)\zeta]^3} I_5^H, \\ v(\zeta) &= \mu_0 + \frac{3c\mu_0(\zeta-\mu_0)}{(2+c)\mu_0+(1-c)\zeta}, \\ w(\zeta) &= \mu_0 + \frac{9c^2(\zeta-\mu_0)^2\mu_0}{[(2+c)\mu_0+(1-c)\zeta]^2}\left[\frac{4}{45} - \frac{81c^{11/25}}{500} + \frac{\mu_0}{c(\zeta-\mu_0)}\right]. \end{aligned}$$

Remark 10. *The two material functions and three material parameters in (60) and their calibration.* The free-energy function (60) comprises two material functions, $\Psi_{\mathtt{m}}(I_1)$ and $\mathcal{S}_{\mathtt{p}}(I_5^H)$, and three material parameters, $\mu_{\mathtt{p}} \geq \mu_0$, $m_{\mathtt{p}}^s \geq 0$, and $c \in [0,1]$; recall that the material functions $\Psi_{\mathtt{m}}(I_1)$ and $\mathcal{S}_{\mathtt{p}}(I_5^H)$ are subject to the linearization, convexity, and growth conditions (25)–(27). Physically, similarly to the model (45) for MREs containing iron particles, the functions $\Psi_{\mathtt{m}}(I_1)$ and $\mathcal{S}_{\mathtt{p}}(I_5^H)$ describe the elastic and magnetization responses of the elastomeric matrix and ferrofluid particles making up the MRE, with $\mu_{\mathtt{p}}$, $m_{\mathtt{p}}^s$, and c describing the initial permeability, magnetization saturation, and volume fraction of the ferrofluid particles.

As it was the case for the model (45), no calibration is needed of (60) when all five inputs $\Psi_{\mathtt{m}}(I_1)$, $\mathcal{S}_{\mathtt{p}}(I_5^H)$, $\mu_{\mathtt{p}}$, $m_{\mathtt{p}}^s$, c happen to be known from the fabrication process of the given MRE of interest. When only some or even none of them are known, those can be readily calibrated from uniaxial tension and magnetization tests on the MRE in precisely the same manner outlined in Remark 6.

Remark 11. *The limits when $c = 0$ and $c = 1$.* In the absence of ferrofluid particles when $c = 0$, the free-energy function (60) reduces to that of the elastomer (23). In the opposite limiting case when $c = 1$, the free-energy function (60) reduces to that of the ferrofluid particles (49).

Remark 12. *The constitutive relations (2).* The constitutive relations (2) implied by the free-energy function (60) are given by

$$\begin{aligned} \mathbf{S} &= 2(1-c)^{5/3}\Psi_{\mathtt{m}}'\left((1-c)^{2/3}(I_1-3)+3\right)\mathbf{F} + \left[w(\zeta) + c\left(2\mathcal{S}_{\mathtt{p}}'(\mathcal{J}_5) - \zeta\right)\frac{\partial \mathcal{J}_5}{\partial I_5^H}\right]\mathbf{F}^{-T}\mathbf{H}\otimes\mathbf{F}^{-1}\mathbf{F}^{-T}\mathbf{H} - p\mathbf{F}^{-T}, \\ \mathbf{B} &= \left[v(\zeta) - w(\zeta) + c\left(2\mathcal{S}_{\mathtt{p}}'(\mathcal{J}_5) - \zeta\right)\frac{\partial \mathcal{J}_5}{\partial I_4^H}\right]\mathbf{H} + \left[w(\zeta) + c\left(2\mathcal{S}_{\mathtt{p}}'(\mathcal{J}_5) - \zeta\right)\frac{\partial \mathcal{J}_5}{\partial I_5^H}\right]\mathbf{F}^{-1}\mathbf{F}^{-T}\mathbf{H}, \end{aligned} \tag{61}$$

where the derivatives $\partial \mathcal{J}_5/\partial I_4^H$ and $\partial \mathcal{J}_5/\partial I_5^H$ are spelled out in Appendix A.2 and where p stands for an arbitrary hydrostatic pressure.

Remark 13. *The corresponding* $(\mathbf{F},\mathbf{B})$ *version.* For the special case when the magnetic behavior of the ferrofluid particles is linear — that is, when $\mathcal{S}_{\mathtt{p}}(I_5^H) = -\mu_{\mathtt{p}} I_5^H/2$ — the free-energy function (60) admits an explicit partial inversion of its argument $\mathbf{H}$ in favor of $\mathbf{B}$. Precisely, for such a case the partial Legendre transform (5) of (60) is given by

$$W^B(\mathbf{F},\mathbf{B}) = (1-c)\Psi_{\mathtt{m}}\left((1-c)^{2/3}(I_1-3)+3\right) + \frac{1}{2w(\mu_{\mathtt{p}})}\left[\frac{I_5^B + n^2 I_4^B + n\left(I_1 I_5^B - I_6^B\right)}{1+n^3+n^2 I_2 + n I_1}\right],$$

where $n = (v(\mu_{\mathtt{p}}) - w(\mu_{\mathtt{p}}))/w(\mu_{\mathtt{p}})$ and where we recall again that the invariants I_2 and I_4^B, I_5^B, I_6^B are given by $(10)_2$ and (12) in terms of the deformation gradient $\mathbf{F}$ and the Lagrangian magnetic induction $\mathbf{B}$. More generally, however, the free-energy function (60) does not admit an explicit inversion.

7. Assessment of the proposed models

This section provides an assessment of the proposed explicit models by direct comparisons with the homogenization solutions (21) and (47). Subsection 7.1 presents basic quantitative comparisons between the free energies (45), (60) and (21), (47) for a large range of deformations gradients $\mathbf{F}$ and Lagrangian magnetic fields $\mathbf{H}$. On the other hand, Subsection 7.2 presents comparisons between the responses predicted by (45), (60) and that predicted by (21), (47) for the magnetostriction of a spherical specimen made of an MRE subject to a remotely applied uniform magnetic field.

Results are reported for MREs made of a silicone elastomer, whose stored-energy function Ψ is characterized by (29) and the material parameters listed in Table 1, filled with iron and ferrofluid particles whose magnetization saturation function $\mathcal{S}_{\mathtt{p}}$ is characterized by (30) with the material parameters listed in Table 1. We remark that the material parameters G_1, G_2, α_1, α_2 in Table 1 describe a common soft silicone elastomer (Poulain et al., 2017). On the other hand, the material parameters $\mu_{\mathtt{p}}$ and $m_{\mathtt{p}}^s$ in Table 1 are representative of typical iron particles (Psarra et al., 2017) and of ferrofluid particles.

Table 1: Material parameters in the stored-energy function (29) and in the magnetization saturation function (30) used to describe the underlying (silicone) elastomer and the iron and ferrofluid particles making up the MREs under investigation

Material	α_1	α_2	G_1 (kPa)	G_2 (kPa)	$\mu_{\mathtt{p}}$	$\mu_0 m_{\mathtt{p}}^s$ (T)
Silicone	-1.02103	1.39107	18.57	31.92		
Iron					$31\mu_0$	2.5
Ferrofluid					$5\mu_0$	0.825

7.1. Comparisons between the proposed free energies (45), (60) and the homogenization solutions (21), (47)

We begin by presenting quantitative comparisons between the free energies (45), (60) and (21), (47) for a wide range of deformations gradients $\mathbf{F}$ and Lagrangian magnetic fields $\mathbf{H}$. Since these free energies possess the same mechanical part $W_{mech}(I_1)$, we only report results for their respective combinations $W - W_{mech}$ that are all independent of I_1 and depend only on the invariants I_4^H and I_5^H. Here, it is appropriate to note that the accuracy of the homogenization solutions (21) and (47) has already been demonstrated — within the mathematically analogous setting of elastic dielectric composites, for a large class of matrix and particle behaviors and for volume fractions up to $c = 0.20$ — for finite deformations and finite magnetic fields via direct comparisons with full-field simulations in Section 6 of Lefèvre and Lopez-Pamies (2017a).

Plots of the free energies (21) and (45) are shown in Fig. 2 for an MRE containing (a) $c = 0.1$ and (b) $c = 0.2$ volume fraction of iron particles. Both plots indicate a good qualitative agreement between the phenomenological free energy (45) and the homogenization solution (21). Comparisons of the same type, not shown here for brevity, indicate that this remains the case for volume fractions $c \in [0, 0.3]$ over a wide

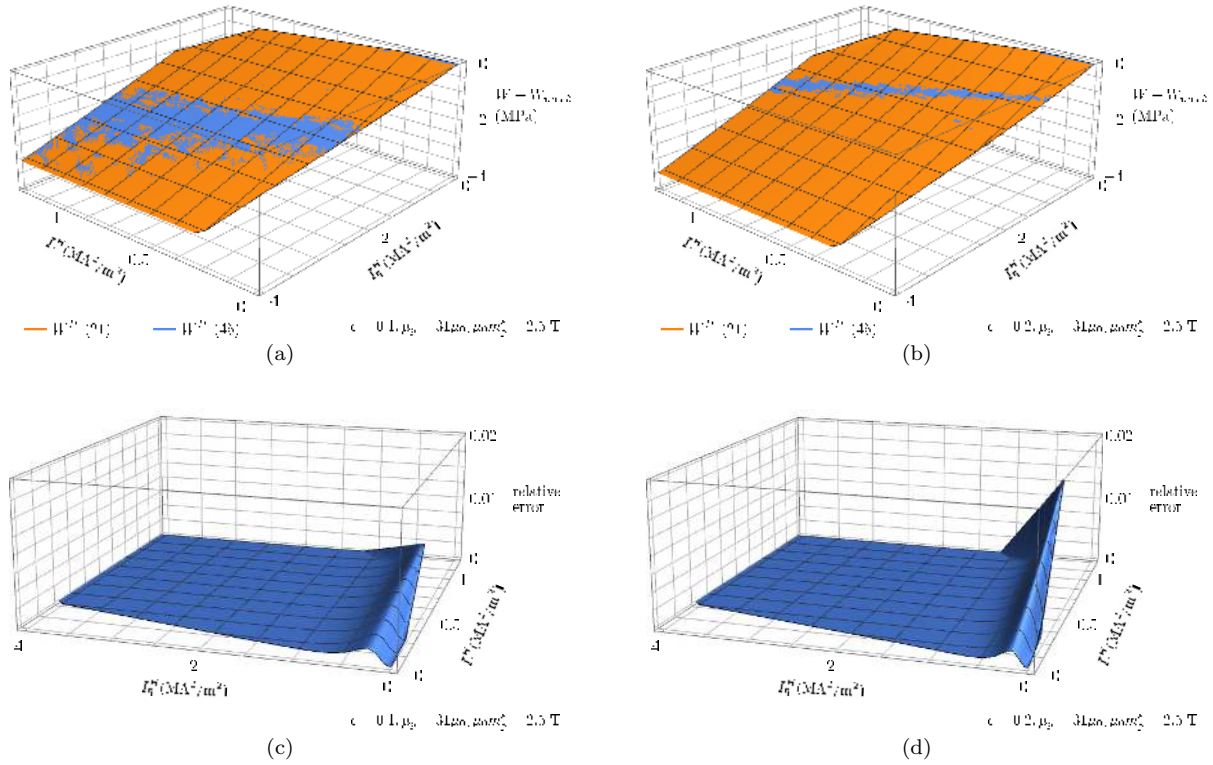

Figure 2: Plots (a)-(b) of the combination $W - W_{mech}$ of the free energies (21), (45) and (c)-(d) of the local relative error in the 1-norm between the phenomenological free energies (45) and the homogenization solution (21). Results are plotted over a wide range of physically meaningful values of the invariants I_4^H, I_5^H and correspond to an MRE containing (a), (c) $c = 0.1$ and (b), (d) $c = 0.2$ volume fraction of iron particles with material parameters listed in Table 1.

range of physically relevant values of the initial permeability μ_p and magnetization saturation m_p^s of the iron particles.

In order to gain quantitative insight into these comparisons, the local relative error in the 1-norm (i.e., the absolute value of the pointwise relative difference) between the phenomenological free energy (45) and the homogenization solution (21) are plotted in Fig. 2 for the same MRE with (c) $c = 0.1$ and (d) $c = 0.2$ volume fraction of iron particles. For $c = 0.1$, Fig. 2(c) reveals that the phenomenological free energy (45) remains within 1.0% of the homogenization solution (21) over the range of values considered for the invariants I_4^H and I_5^H. Figure 2(d) for $c = 0.2$ shows the same trend as Fig. 2(c), now with respective relative error below 1.5%. Here as well, comparisons of the same type not reported here for brevity have shown similar trends for volume fractions $c \in [0, 0.3]$ over a wide range of physically relevant values of the initial permeability μ_p and magnetization saturation m_p^s of the iron particles.

Analogous plots of the free energies (47) and (60) are shown in Fig. 3 for an MRE containing (a) $c = 0.1$ and (b) $c = 0.2$ volume fraction of ferrofluid particles. Both plots indicate a good qualitative agreement between the phenomenological free energy (60) and the homogenization solution (47). Comparisons of the same type, also not shown here for brevity, indicate that this remains the case for volume fractions $c \in [0, 0.3]$ over a wide range of physically relevant values of the initial permeability μ_p and magnetization saturation m_p^s of the ferrofluid particles.

Again, in order to gain quantitative insight into these comparisons, the local relative error in the 1-norm (i.e., the absolute value of the pointwise relative difference) between the phenomenological free energy (60) and the homogenization solution (47) are plotted in Fig. 3 for the same MRE with (c) $c = 0.1$ and (d) $c = 0.2$ volume fraction of ferrofluid particles. For $c = 0.1$, Fig. 3(c) reveals that the phenomenological free energy (60) remains within 1.5% of the homogenization solution (47) over the range of values considered for

the invariants I_4^H and I_5^H. Figure 3(d) for $c = 0.2$ shows the same trend as Fig. 3(c), now with respective relative error below 2.0%. Here as well, comparisons of the same type not reported here for brevity have shown similar trends for volume fractions $c \in [0, 0.3]$ over a wide range of physically relevant values of the initial permeability μ_{p} and magnetization saturation m_{p}^s of the ferrofluid particles.

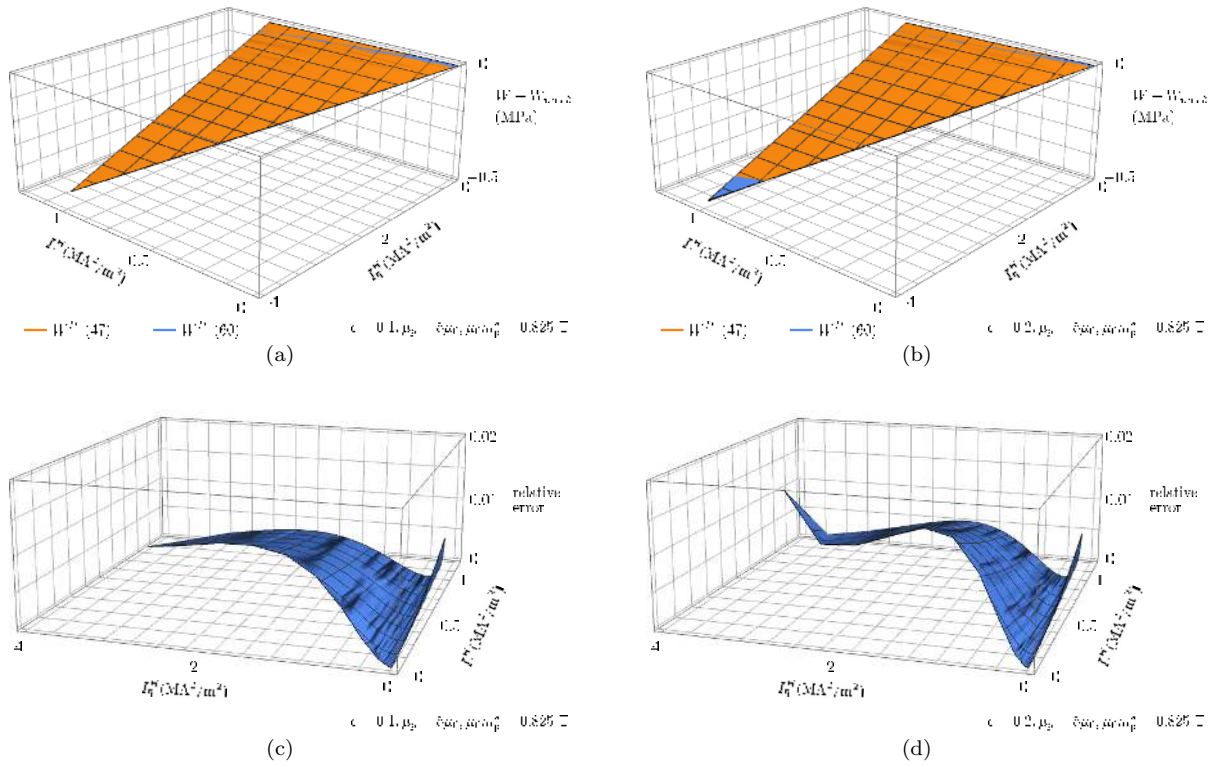

Figure 3: Plots (a)-(b) of the combination $W - W_{mech}$ of the free energies (47), (60) and (c)-(d) of the local relative error in the 1-norm between the phenomenological free energies (60) and the homogenization solution (47). Results are plotted over a wide range of physically meaningful values of the invariants I_4^H, I_5^H and correspond to an MRE containing (a), (c) $c = 0.1$ and (b), (d) $c = 0.2$ volume fraction of ferrofluid particles with material parameters listed in Table 1.

7.2. Comparisons for the magnetostriction response of a spherical MRE specimen

In order to further and more critically assess the proposed explicit models, we now report comparisons between the responses predicted by (45), (60) and those predicted by (21), (47) for the magnetostriction of spherical specimens made of MREs containing iron and ferrofluid particles subject to a remotely applied uniform magnetic field. In addition to its fundamental and practical relevance (Brown, 1966; Diguet, 2010), such a boundary-value problem allows to probe the difference between the proposed models (45), (60) and the homogenization solutions (21), (47) over physically meaningful deformations and magnetic fields that are realizable with conventional equipment (Lefèvre et al., 2017).

We follow the approach of Lefèvre et al. (2017) wherein, for computational expediency, numerical solutions in the specimen and surrounding space — assumed to be air — are generated on a spatial domain of sufficiently large but finite extent, and not on $\mathbb{R}^3$ entirely. While full details of this approach can be found in Section 6 in (Lefèvre et al., 2017), it is appropriate to mention here that (*i*) the finite domain of computation is comprised of the spherical MRE specimen surrounded by an air-filled thick spherical shell subjected on its external surface to the affine boundary conditions $\mathbf{x} = \mathbf{X}$ and $\psi = -\mathbf{H}_\infty \cdot \mathbf{X}$ (see Fig. 4(a)), (*ii*) the surrounding air is treated as a highly compressible magnetoelastic material with vanishingly small mechanical stiffness, and (*iii*) the numerical solutions are generated by means of a conforming axisymmet-

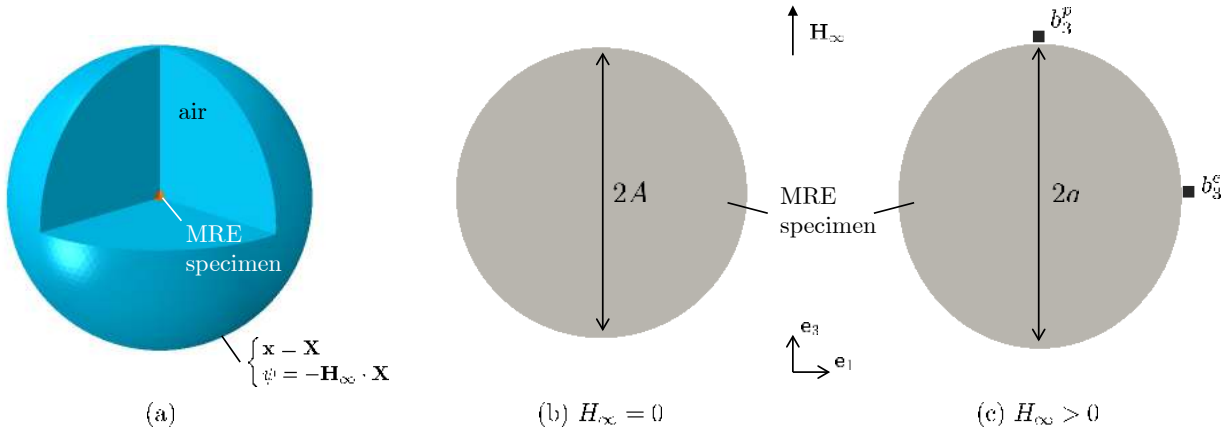

Figure 4: (a) Schematic of the finite domain utilized to generate numerical solutions for the boundary-value problem (19). The air domain is defined by a spherical shell of initial outer radius that is twenty times that of the MRE specimen. Schematics of a spherical MRE specimen of initial radius A in (b) its initial configuration and (c) its deformed configuration indicating the poles utilized to compute the overall magnetostriction a/A and points in the air adjacent to the specimen utilized to compute the overall magnetization $(b_3^p - b_3^e)/\mu_0$.

ric 7-node hybrid triangular finite element discretization that leverages the axial symmetry of the problem around the direction, say $\mathbf{e}_3$, of the applied magnetic field $\mathbf{H}_\infty = H_\infty \mathbf{e}_3$.

By providing *pointwise* solutions for the deformation and magnetic fields in the MRE specimen and surrounding air, this approach also allows to extract *global* information about the deformation and magnetization of the specimen as would be done experimentally. Following standard approaches in the literature, the overall magnetostriction stretch of the specimen is simply defined here as the stretch of the distance between the two poles of the specimen in the $\mathbf{e}_3$ direction; see Fig. 4(b),(c). By leveraging the continuity equations (13)–(14), the overall magnetization of the *specimen* is defined as $(b_3^p - b_3^e)/\mu_0$ where b_3^p and b_3^e are the $\mathbf{e}_3$-components of the Eulerian magnetic induction $\mathbf{b}$ — accessible experimentally with Hall probes (see, e.g., Bodelot et al. (2018)) — probed in the *air* immediately adjacent to the pole and equator of MRE specimen, respectively; see Fig. 4(c). Due to the non-uniform spatial variations of the deformation and magnetic fields in the specimen, we emphasize here that these overall magnetostriction and overall magnetization do *not* correspond in general to the average of the local magnetostriction and magnetization in the specimen. Rather, they correspond to *structural* — and not just material — information about the response of the MRE specimen that is accessible experimentally and provide, in addition to the pointwise solutions, another way of assessing the proposed explicit models.

Results for MREs containing iron particles. Figures 5-6 present contour plots in the $\mathbf{e}_1$-$\mathbf{e}_3$ plane of the local component $F_{33}(\mathbf{X})$ of the deformation gradient and of the local component $m_3(\mathbf{x})$ of the magnetization over spherical specimens made of MREs characterized by (a)–(c) the proposed phenomenological model (45) and (d)–(f) the homogenization solution (21), and containing $c = 0.222$ volume fraction of iron particles with material properties listed in Table 1. The contours in Fig. 5 are shown over the undeformed configuration of the specimen as implied by the argument $\mathbf{X}$ of $F_{33}(\mathbf{X})$, while the contours in Fig. 6 are shown over the deformed configuration of the specimen as implied by the argument $\mathbf{x}$ of $m_3(\mathbf{x})$. Further, the contours correspond to the magnitudes $H_\infty = 0.5$, 1.0, 1.5 MA/m of the remotely applied magnetic field $\mathbf{H}_\infty$, and the color scale bars in each of them indicate the corresponding variation of the quantity of interest from its minimum to its maximum.

A quick glance at Figs. 5-6 suffices to recognize the good agreement between the response predicted by the proposed phenomenological model (45) and that by the homogenization solution (21). It is also clear from Fig. 5 that the local deformation gradient is highly heterogeneous, with regions in tension in the core of the specimen and regions in compression at its poles, while Fig. 6 indicates that the local magnetization is much more uniform across the specimen. This implies that the material magnetization response of the

MRE can be accurately measured as described above for spherical specimens; the same is *not* true in general for cylindrical specimens (Lefèvre et al., 2017).

Additional insight into the differences between the proposed phenomenological model (45) and the homogenization solution (21) is obtained by plotting in Fig. 7 (a) the overall magnetostriction and (b) the overall magnetization — as defined above — as functions of the magnitude H_∞ of the remotely applied magnetic field for three volume fractions $c = 0.087,\ 0.16,\ 0.222$ of iron particles. As expected from the fact that, by construction (see Section 4), for arbitrary deformations and all volume fractions, the proposed model (45) agrees exactly with the homogenization solution (21) for infinitely small and infinitely large magnetic fields, the two sets predictions for the overall magnetostriction and overall magnetization shown in Fig. 7 agree in these limiting ranges of applied magnetic fields for the three volume fractions considered. As expected further from the local good qualitative agreement shown in Figs. 5-6 for intermediate values of H_∞, the two predictions of the proposed model (45) are in good qualitative agreement with those predicted by the homogenization solution (21), with some quantitative differences for the overall magnetostriction in this range of applied magnetic fields. It is expected that these quantitative differences may be reduced by employing the model (31) in the proposed model (45) with an appropriate value of the parameter γ_{p}. From a quantitative perspective, the specimens with volumes fractions $c = 0.087,\ 0.16,\ 0.222$ of iron particles reach a saturated magnetostriction of about 1.01, 1.04, 1.06 and saturated magnetization of about 0.17, 0.31, 0.43 MA/m, respectively, for applied magnetic fields $H_\infty \geq 1.5$ MA/m.

Results for MREs containing ferrofluid particles. Similar to Figs. 5-6 for the case of iron particles, Figs. 8-9 present contour plots in the $\mathbf{e}_1$-$\mathbf{e}_3$ plane of the local component $F_{33}(\mathbf{X})$ of the deformation gradient and of the local component $m_3(\mathbf{x})$ of the magnetization over spherical specimens made of MREs characterized by (a)–(c) the proposed phenomenological model (60) and (d)–(f) the homogenization solution (47), and containing $c = 0.222$ volume fraction of ferrofluid particles with material properties listed in Table 1. The contours in Fig. 5 are shown over the undeformed configuration of the specimen as implied by the argument $\mathbf{X}$ of $F_{33}(\mathbf{X})$, while the contours in Fig. 6 are shown over the deformed configuration of the specimen as implied by the argument $\mathbf{x}$ of $m_3(\mathbf{x})$. The contours correspond to the magnitudes $H_\infty = 0.5,\ 1.0,\ 1.5$ MA/m of the remotely applied magnetic field $\mathbf{H}_\infty$, and the color scale bars in each of them indicate the corresponding variation of the quantity of interest from its minimum to its maximum.

A quick glance at Figs. 8-9 suffices to recognize the good agreement between the response predicted by the proposed phenomenological model (60) and that by the homogenization solution (47). It is also plain from Fig. 8 that the local deformation gradient is also highly heterogeneous, though less so than for the case of iron particles as the specimen made of MRE with ferrofluid particles is locally only tension. Similar to Fig. 6, Fig. 9 indicates that the local magnetization is almost uniform across the specimen.

Here again, additional insight into the differences between the proposed phenomenological model (60) and the homogenization solution (47) is obtained by plotting in Fig. 10 (a) the overall magnetostriction and (b) the overall magnetization — as defined above — as functions of the magnitude H_∞ of the remotely applied magnetic field for three volume fractions $c = 0.087,\ 0.16,\ 0.222$ of ferrofluid particles. The predictions from the proposed phenomenological model (60) for the overall magnetostriction and overall magnetization are in good qualitative and quantitative agreement with those of the homogenization solution (47) over the entire range of applied magnetic field. This stems again from the fact that, by construction (see Section 6), the proposed model (60) agrees exactly — for arbitrary deformations and all volume fractions — with the homogenization solution (47) for infinitely small and infinitely large magnetic fields, and from the local good qualitative agreement shown on Figs. 8-9 for intermediate values of H_∞. Quantitatively, the specimens with $c = 0.087,\ 0.16,\ 0.222$ reach a magnetostriction of about 1.14, 1.35, 1.75, much larger than corresponding specimens with iron particles, and magnetization of about 0.06, 0.10, 0.15 MA/m, respectively, at $H_\infty = 2.0$ MA/m. It is clear from Fig.10(a) that MREs containing ferrofluid particles hold promising potential for practical use in MRE-based devices leveraging their magnetostrictive capabilities.

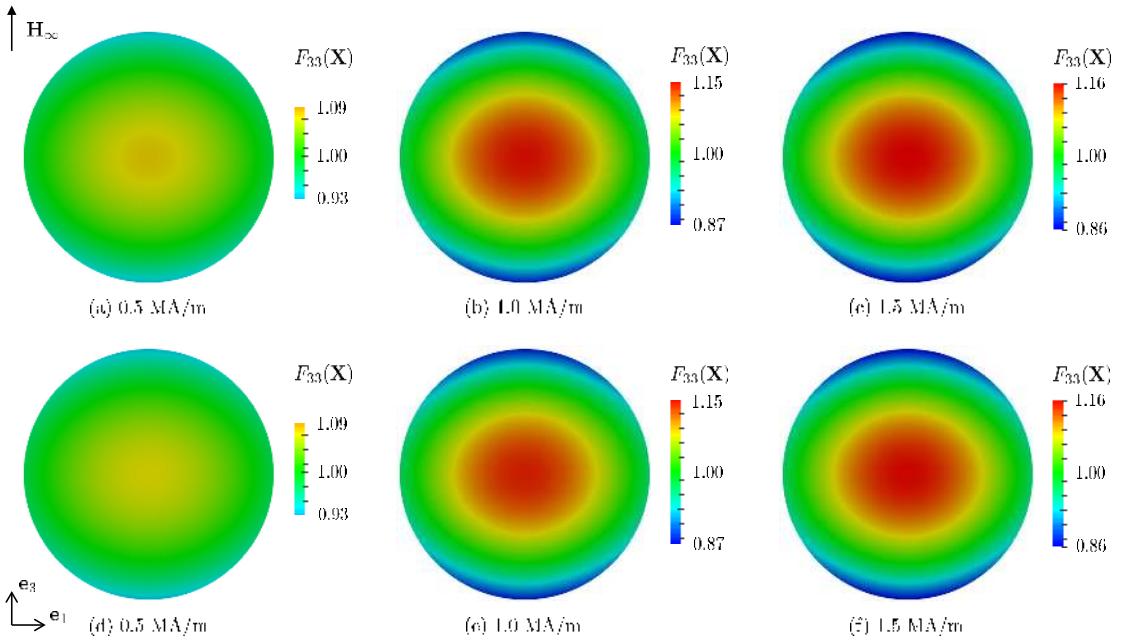

Figure 5: Contour plots of the component $F_{33}(\mathbf{X})$ of the deformation gradient over spherical specimens made of a MRE characterized by (a)–(c) the proposed model (45) and (d)–(f) the homogenization solution (21), and containing $c = 0.222$ volume fraction of iron particles. The contours correspond to the remotely applied magnetic field $\mathbf{H}_\infty = H_\infty \mathbf{e}_3$ with H_∞=0.5, 1.0, 1.5 MA/m and are shown over the undeformed configuration of the specimens.

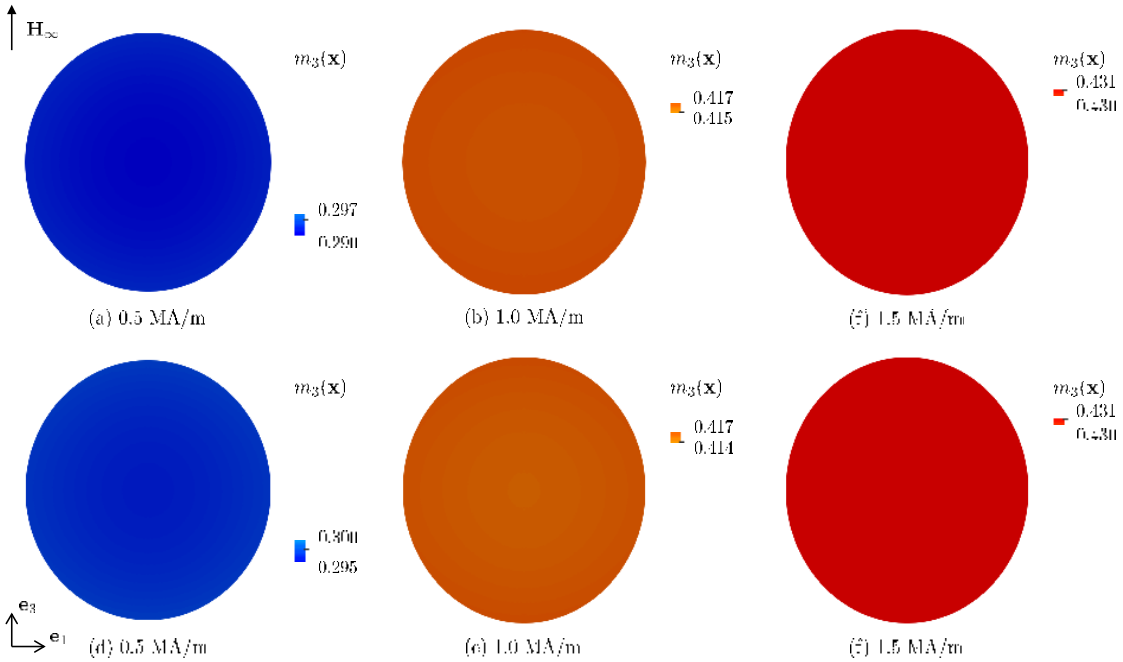

Figure 6: Contour plots of the component $m_3(\mathbf{x})$ of the magnetization over spherical specimens made of a MRE characterized by (a)–(c) the proposed model (45) and (d)–(f) the homogenization solution (21), and containing $c = 0.222$ volume fraction of iron particles. The contours correspond to the remotely applied magnetic field $\mathbf{H}_\infty = H_\infty \mathbf{e}_3$ with H_∞=0.5, 1.0, 1.5 MA/m and are shown over the deformed configuration of the specimens.

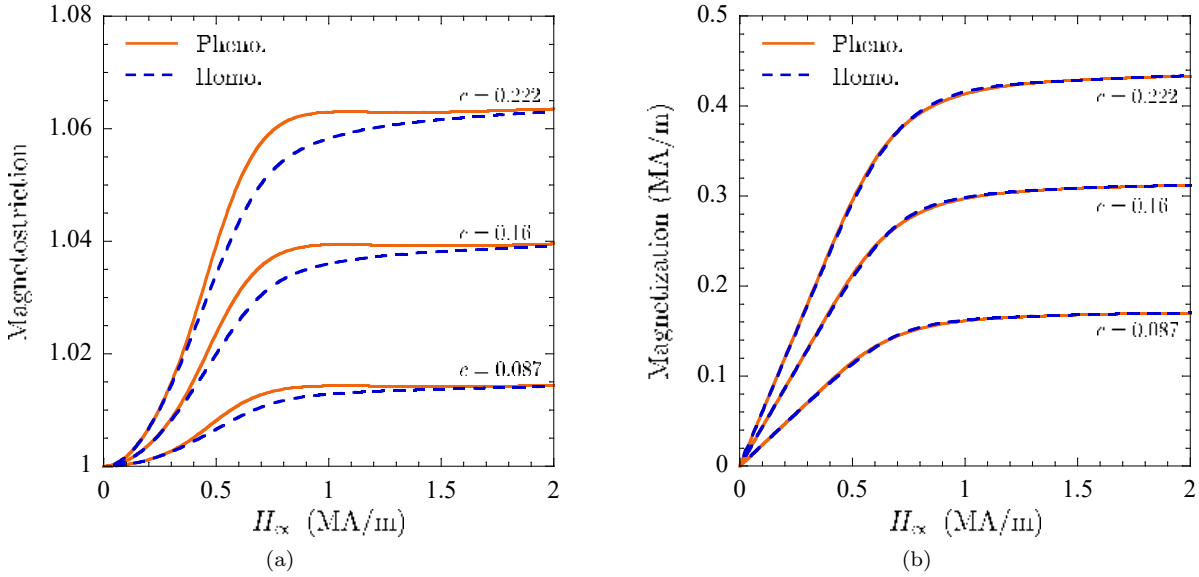

Figure 7: (a) Overall magnetostriction and (b) overall magnetization of spherical specimens made of a MRE characterized by the phenomenological model (45) labelled "Pheno.", and the homogenization solution (21) labelled "Homo.", and containing $c = 0.087$, 0.16, 0.222 volume fraction of iron particles.

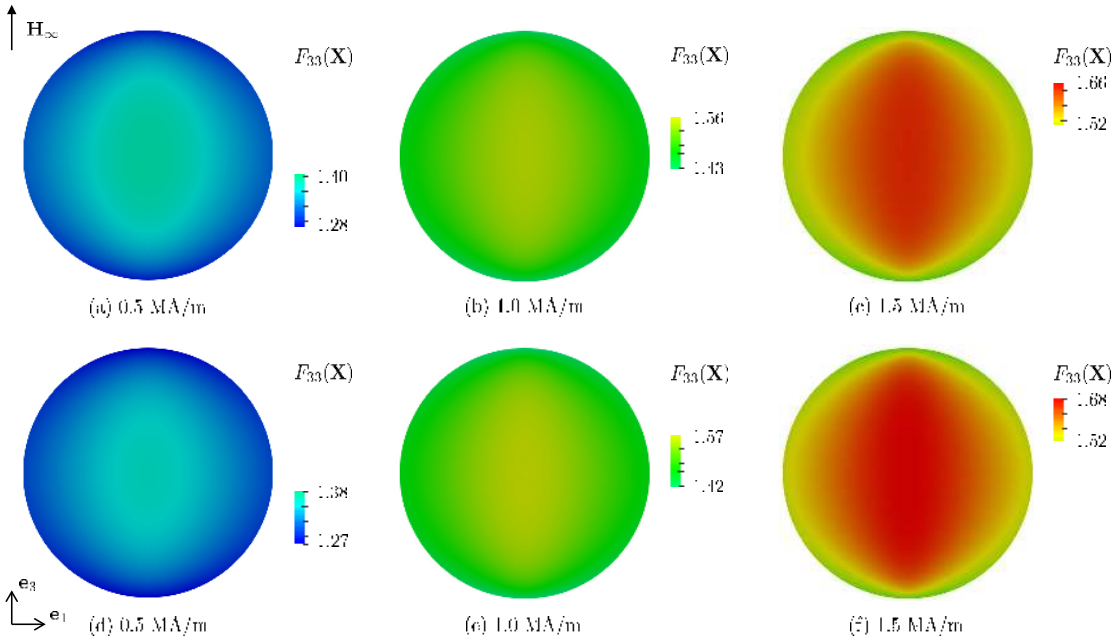

Figure 8: Contour plots of the component $F_{33}(\mathbf{X})$ of the deformation gradient over spherical specimens made of a MRE characterized by (a)–(c) the proposed model (60) and (d)–(f) the homogenization solution (47), and containing $c = 0.222$ volume fraction of ferrofluid particles. The contours correspond to the remotely applied magnetic field $\mathbf{H}_\infty = H_\infty \mathbf{e}_3$ with H_∞=0.5, 1.0, 1.5 MA/m and are shown over the undeformed configuration of the specimens.

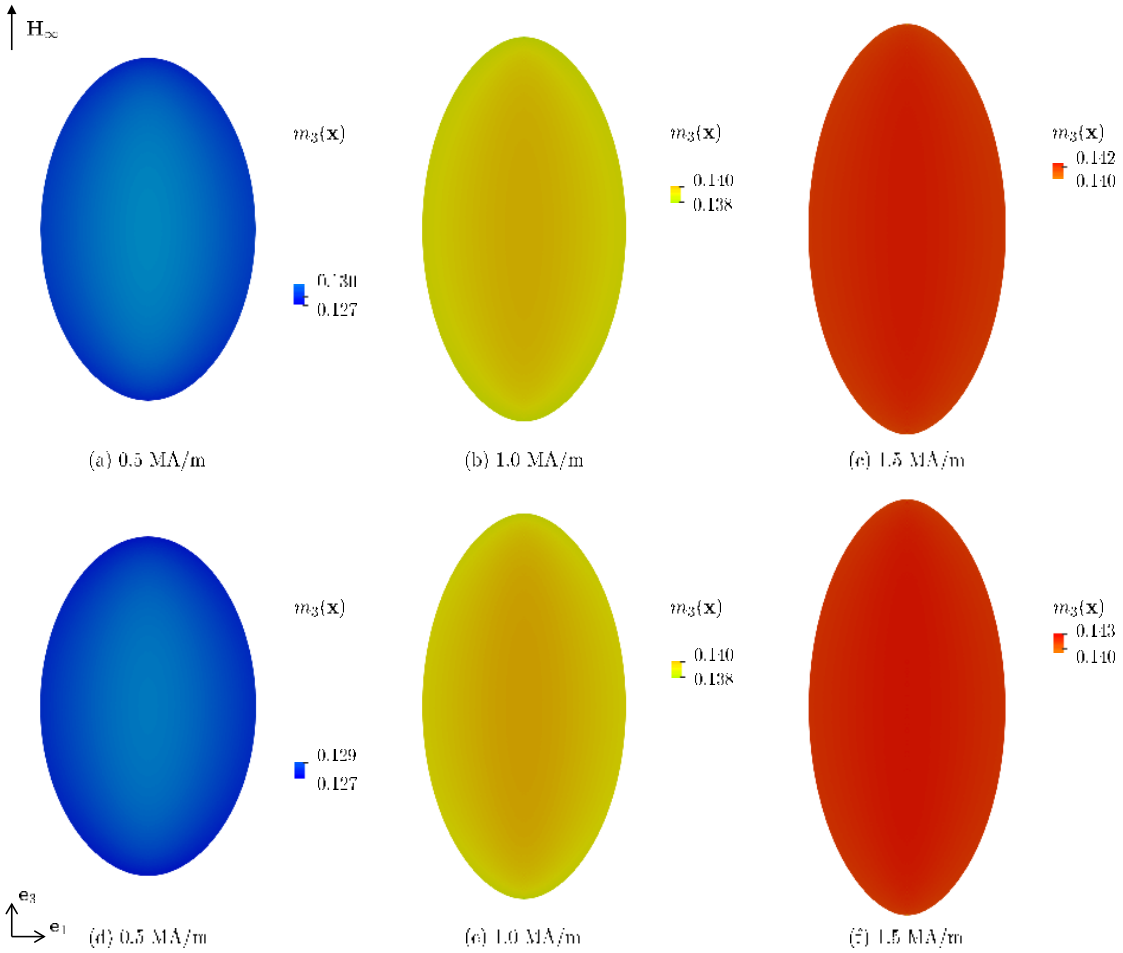

Figure 9: Contour plots of the component $m_3(\mathbf{x})$ of the magnetization over spherical specimens made of a MRE characterized by (a)–(c) the proposed model (45) and (d)–(f) the homogenization solution (21), and containing $c = 0.222$ volume fraction of ferrofluid particles. The contours correspond to the remotely applied magnetic field $\mathbf{H}_\infty = H_\infty \mathbf{e}_3$ with H_∞=0.5, 1.0, 1.5 MA/m and are shown over the deformed configuration of the specimens.

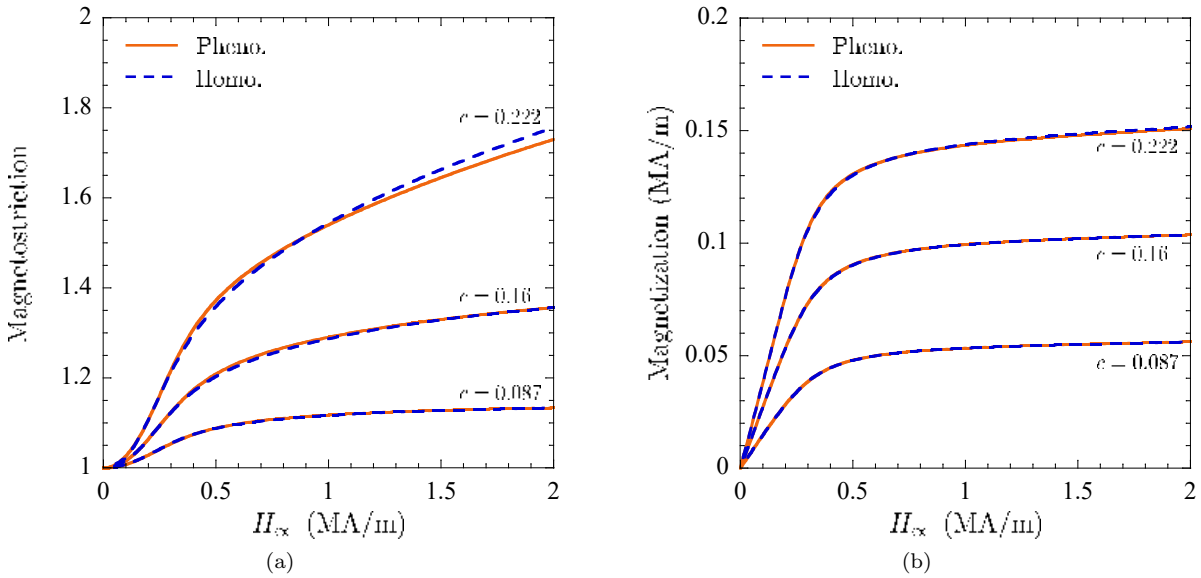

(a) (b)

Figure 10: (a) Overall magnetostriction and (b) overall magnetization of spherical specimens made of a MRE characterized by the phenomenological model (60) labelled "Pheno.", and the homogenization solution (47) labelled "Homo.", and containing $c = 0.087$, 0.16, 0.222 volume fraction of ferrofluid particles.

Acknowledgments

VL acknowledges the support for this work through the computational resources and staff contributions provided for the Quest high performance computing facility at Northwestern University which is jointly supported by the Office of the Provost, the Office for Research, and Northwestern University Information Technology. OLP acknowledges the support for this work by the National Science Foundation, United States through the Grant CMMI–1661853.

Appendix A: The derivatives entering the constitutive relations (46) and (61)

A.1. The partial derivatives entering in (46)

The derivatives $\partial\mathcal{I}_5/\partial I_4^H$ and $\partial\mathcal{I}_5/\partial I_5^H$ that enter in the constitutive relations (46) implied by the free-energy function (45) are given by

$$\frac{\partial\mathcal{I}_5}{\partial I_4^H}=-\frac{54c(1-c)(\xi-\mu_0)\mu_0^2}{5[(2+c)\mu_0+(1-c)\xi]^3}$$

and

$$\begin{aligned}\frac{\partial\mathcal{I}_5}{\partial I_5^H}=&\left[\frac{54c(1-c)[(5-2c)\mu_0-2(1-c)\xi]\mu_0^2}{5[(2+c)\mu_0+(1-c)\xi]^4}I_4^H+\frac{18(1-c)[\left(10-10c+6c^2\right)\mu_0+\left(5+c-6c^2\right)\xi]\mu_0^2}{5[(2+c)\mu_0+(1-c)\xi]^4}I_5^H\right]\times\\&\frac{2a_0+3a_1(I_5^H)^{1/2}+4a_2I_5^H+(\xi-\mu_{\mathrm{p}})\left(a_4(I_5^H)^{-1/2}+2a_5+3a_6(I_5^H)^{1/2}+4a_7I_5^H\right)}{2[a_3+a_4(I_5^H)^{1/2}+a_5I_5^H+a_6(I_5^H)^{3/2}+a_7(I_5^H)^2]}+\\&\frac{9[(10-c+6c^2)\mu_0+(5+c-6c^2)\xi]\mu_0^2}{5[(2+c)\mu_0+(1-c)\xi]^3}.\end{aligned}$$

A.2. The partial derivatives entering in (61)

The derivatives $\partial\mathcal{J}_5/\partial I_4^H$ and $\partial\mathcal{J}_5/\partial I_5^H$ that enter in the constitutive relations (61) implied by the free-energy function (60) are given by

$$\frac{\partial\mathcal{J}_5}{\partial I_4^H}=\frac{3\left(1500-1900c+729c^{36/25}\right)(\zeta-\mu_0)\mu_0^2}{250[(2+c)\mu_0+(1-c)\zeta]^3}$$

and

$$\begin{aligned}\frac{\partial\mathcal{J}_5}{\partial I_5^H}=&\frac{3\mu_0^2[\left(3000-1150c+729c^{36/25}\right)\mu_0-\left(750-1150c+729c^{36/25}\right)\zeta]}{250[(2+c)\mu_0+(1-c)\zeta]^3}+\left[\frac{3\left(750-1150c+729c^{36/25}\right)\mu_0^2}{125[(2+c)\mu_0+(1-c)\zeta]^3}I_5^H-\right.\\&\left.\frac{27\left(1500-1900c+729c^{36/25}\right)\mu_0^3}{250[(2+c)\mu_0+(1-c)\zeta]^4}I_5^H+\frac{3\left(1500-1900c+729c^{36/25}\right)[(5-2c)\mu_0-2(1-c)\zeta]\mu_0^2}{250[(2+c)\mu_0+(1-c)\zeta]^4}I_4^H\right]\times\\&\frac{2a_0+3a_1(I_5^H)^{1/2}+4a_2I_5^H+(\zeta-\mu_{\mathrm{p}})\left(a_4(I_5^H)^{-1/2}+2a_5+3a_6(I_5^H)^{1/2}+4a_7I_5^H\right)}{2[a_3+a_4(I_5^H)^{1/2}+a_5I_5^H+a_6(I_5^H)^{3/2}+a_7(I_5^H)^2]}\end{aligned}$$

References

Arruda, E. M., Boyce, M. C., 1993. A three-dimensional constitutive model for the large stretch behavior of rubber elastic materials. J Mech Phys Solids 41, 389–412.

Bodelot, L., Voropaieff, J.-P., Pössinger, T., Feb 2018. Experimental investigation of the coupled magneto-mechanical response in magnetorheological elastomers. Exp Mech 58 (2), 207–221.
URL https://doi.org/10.1007/s11340-017-0334-7

Brown, W. F., 1966. Magnetoelastic interactions. Springer-Verlag, New York.

Danas, K., 2017. Effective response of classical, auxetic and chiral magnetoelastic materials by use of a new variational principle. J. Mech. Phys. Solids 105, 25–53.
Danas, K., Kankanala, S., Triantafyllidis, N., 2012. Experiments and modeling of iron-particle-filled magnetorheological elastomers. J. Mech. Phys. Solids 60 (1), 120–138.
URL http://www.sciencedirect.com/science/article/pii/S0022509611001736
Diguet, G., 2010. Huge magnetostriction of magneto-rheological composite. Ph.D. thesis, Université de Grenoble.
Dorfmann, A., Ogden, R., 2004. Nonlinear magnetoelastic deformations of elastomers. Acta Mechanica 167 (1-2), 13–28.
URL https://doi.org/10.1007/s00707-003-0061-2
Gent, A. N., 1996. A new constitutive relation for rubber. Rubber Chem. Technol. 69, 59–61.
Kankanala, S. V., Triantafyllidis, N., 2004. On finitely strained magnetorheological elastomers. J. Mech. Phys. Solids 52 (12), 2869 – 2908.
URL http://www.sciencedirect.com/science/article/B6TXB-4D5P2GW-1/2/54fb91d5b0a08991f9819e91ab1690b2
Keip, M.-A., Rambausek, M., 2015. A multiscale approach to the computational characterization of magnetorheological elastomers. Int J Numer Methods Eng 7, 23–32, nme.5178.
URL http://dx.doi.org/10.1002/nme.5178
Kittel, C., 2004. Introduction to Solid State Physics. Wiley.
Lefèvre, V., Danas, K., Lopez-Pamies, O., 2017. A general result for the magnetoelastic response of isotropic suspensions of iron and ferrofluid particles in rubber, with applications to spherical and cylindrical specimens. J. Mech. Phys. Solids 107, 343–364.
URL https://doi.org/10.1016/j.jmps.2017.06.017
Lefèvre, V., Garnica, A., Lopez-Pamies, O., 2019. A weno finite-difference scheme for a new class of hamilton–jacobi equations in nonlinear solid mechanics. https://doi.org/10.1016/j.cma.2019.02.008, 17–44.
URL https://doi.org/10.1016/j.cma.2019.02.008
Lefèvre, V., Lopez-Pamies, O., 2017a. Nonlinear electroelastic deformations of dielectric elastomer composites: II — non-gaussian elastic dielectrics. Journal of the Mechanics and Physics of Solids 99, 438–470.
URL https://doi.org/10.1016/j.jmps.2016.07.005
Lefèvre, V., Lopez-Pamies, O., 2017b. Nonlinear electroelastic deformations of dielectric elastomer composites: I—ideal elastic dielectrics. Journal of the Mechanics and Physics of Solids 99, 409–437.
URL https://doi.org/10.1016/j.jmps.2016.07.004
Leonard, M., Wang, N., Lopez-Pamies, O., Nakamura, T., 2020. The nonlinear elastic response of filled elastomers: Experiments vs. theory for the basic case of particulate fillers of micrometer size. Journal of the Mechanics and Physics of Solids 135, 103781.
URL https://doi.org/10.1016/j.jmps.2019.103781
Lopez-Pamies, O., 2010a. An exact result for the macroscopic response of particle-reinforced neo-hookean solids. Journal of Applied Mechanics 77 (2), 021016.
URL https://doi.org/10.1115/1.3197444
Lopez-Pamies, O., 2010b. A new i_1-based hyperelastic model for rubber elastic materials. C. R. Mecanique 338, 3–11.
URL https://doi.org/10.1016/j.crme.2009.12.007
Lopez-Pamies, O., 2014. Elastic dielectric composites: Theory and application to particle-filled ideal dielectrics. Journal of the Mechanics and Physics of Solids 64, 61–82.
URL https://doi.org/10.1016/j.jmps.2013.10.016
Lopez-Pamies, O., Goudarzi, T., Danas, K., 2013. The nonlinear elastic response of suspensions of rigid inclusions in rubber: Ii - a simple explicit approximation for finite-concentration suspensions. J Mech Phys Solids 61 (1), 19 – 37.
URL http://dx.doi.org/10.1016/j.jmps.2012.08.013
Meddeb, A. B., Tighe, T., Ounaies, Z., Lopez-Pamies, O., 2019. Extreme enhancement of the nonlinear elastic response of elastomer nanoparticulate composites via interphases. Composites Part B 156, 166–173.
URL https://doi.org/10.1016/j.compositesb.2018.08.064
Mukherjee, D., Bodelot, L., Danas, K., 2020. Microstructurally-guided explicit continuum models for isotropic magnetorheological elastomers with iron particles. Under review.
Nedjar, B., 2017. A coupled bem-fem method for finite strain magneto-elastic boundary-value problems. Computational Mechanics 59 (5), 795–807.
Ogden, R. W., 1997. Non-linear Elastic Deformations. Dover.
Pelteret, J.-P., Davydov, D., McBride, A., Vu, D. K., Steinmann, P., 2016. Computational electro-elasticity and magneto-elasticity for quasi-incompressible media immersed in free space. International Journal for Numerical Methods in Engineering 108, 307–1342.
Poulain, X., Lefèvre, V., Lopez-Pamies, O., Ravi-Chandar, K., 2017. Damage in elastomers: Nucleation and growth of cavities, micro-cracks, and macro-cracks. International Journal of Fracture 205, 1–21.
URL https://link.springer.com/article/10.1007%2Fs10704-016-0176-9
Psarra, E., Bodelot, L., Danas, K., 2017. Two-field surface pattern control via marginally stable magnetorheological elastomers. Soft Matter 13, 6576–6584.
URL http://dx.doi.org/10.1039/C7SM00996H
Saxena, P., Pelteret, J.-P., Steinmann, P., 2015. Modelling of iron-filled magneto-active polymers with a dispersed chain-like microstructure. European Journal of Mechanics - A/Solids 50, 132 – 151.
URL http://www.sciencedirect.com/science/article/pii/S0997753814001508
Steigmann, D. J., 2004. Equilibrium theory for magnetic elastomers and magnetoelastic membranes. Int J Non Linear Mech

39 (7), 1193–1216.
URL http://www.sciencedirect.com/science/article/pii/S0020746203001173

Treloar, L. R. G., 1943. The elasticity of a network of long-chain molecules – ii. Trans. Faraday Soc. 39, 241 – 246.
URL https://pubs.rsc.org/en/content/articlelanding/1943/tf/tf9433900241#!divAbstract

Vu, D., Steinmann, P., 2010. A 2-d coupled bem–fem simulation of electro-elastostatics at large strain. Computer Methods in Applied Mechanics and Engineering 199 (17), 1124 – 1133.
URL http://www.sciencedirect.com/science/article/pii/S0045782509004009

Vu, D., Steinmann, P., 2012. On 3-d coupled bem–fem simulation of nonlinear electro-elastostatics. Computer Methods in Applied Mechanics and Engineering 201, 82–90.